Research Article

Journal of Innate Immunity

J Innate Immun
DOI: 10.1159/000355126

Received: August 12, 2013
Accepted after revision: August 19, 2013
Published online: October 29, 2013

Myeloid-Derived Suppressor Cells Confer Tumor-Suppressive Functions on Natural Killer Cells via Polyinosinic:Polycytidylic Acid Treatment in Mouse Tumor Models

Hiroaki Shime Ayako Kojima Akira Maruyama Yusuke Saito
Hiroyuki Oshiumi Misako Matsumoto Tsukasa Seya

Department of Microbiology and Immunology, Graduate School of Medicine, Hokkaido University, Sapporo, Japan

Key Words
Myeloid-derived suppressor cells · Mitochondrial antiviral signaling protein · Tumor immunotherapy · Double-stranded RNA

Abstract
Polyinosinic:polycytidylic acid (poly I:C), a synthetic double-stranded RNA, acts on myeloid cells and induces potent antitumor immune responses including natural killer (NK) cell activation. Myeloid-derived suppressor cells (MDSCs) systemically exist in tumor-bearing hosts and have strong immunosuppressive activity against antitumor effector cells, thereby dampening the efficacy of cancer immunotherapy. Here we tested what happened in MDSCs in poly I:C-treated mice. NK-sensitive syngenic tumor (B16)-bearing C57BL/6 mice were employed for this study. Intraperitoneal poly I:C treatment induced MDSC activation, driving CD69 expression and interferon (IFN)-γ production in NK cells. IFN-γ directly inhibited proliferation of B16 cells. This NK cell priming led to growth retardation of B16 tumors, although no direct tumoricidal activity was induced in NK cells. Mechanistic analysis using KO mice and function-blocking monclonal antibody revealed that MDSCs produced IFN-α via the mitochondrial antiviral signaling protein (MAVS) pathway after in vivo administration of poly I:C, and activated NK cells through the IFNAR pathway. MDSC-mediated NK cell priming was reconstituted by IFN-α in a coculture system. Either the MAVS or IFNAR signaling pathway was required for activation of MDSCs that led to growth retardation of B16 tumor in vivo. The results infer that MDSC is a target of poly I:C to prime NK cells, which exert antitumor activity to NK-sensitive tumor cells.

Introduction

The innate sensing of microbial molecular patterns results in the modulation of the cellular immune system [1–3]. This innate-adaptive linkage closely associates with suppression of infection and tumorigenesis. Many reports showed that polyinosinic:polycytidylic acid (poly I:C), a synthetic pattern of double-stranded RNA, has potent stimulatory effects on immune responses to viral infection and cancer [4–8]. Poly I:C is an agonist for pattern-recognition receptors (PRRs), Toll-like receptor 3 (TLR3) and melanoma differentiation-associated protein 5 (MDA5), which transduce signals to the adaptor molecules TICAM-1 (also known as TRIF) and mitochondrial antiviral signaling protein (MAVS; IPS-1, Cardif, VISA) [9–12]. They differentially modulate the functions of myeloid dendritic cells (DCs) and macrophages, including cytokine/IFN production and expression of surface molecules that drive effector cell activation.

KARGER

E-Mail karger@karger.com
www.karger.com/jin

1662–811X/13/0000–0000$38.00/0

Dr. Tsukasa Seya and Dr. Hiroaki Shime
Department of Microbiology and Immunology
Graduate School of Medicine, Hokkaido University
Kita-ku, Sapporo 060-8638 (Japan)
E-Mail seya-tu@pop.med.hokudai.ac.jp and shime@med.hokudai.ac.jp

TLR3/TICAM-1 and MDA5/MAVS activate the transcription factors, NF-κB and interferon (IFN) regulatory factor 3 (IRF-3), to typically induce type-I IFN. Type-I IFN evokes subsequent activation of the IFNAR pathway, which participates in the induction of IFN-stimulated genes (ISGs) including IRF-7 [13, 14]. IRF-7 further modifies the function of poly I:C by upregulating PRRs. Thus, the activity of poly I:C immediately affects IRF-3-derived genes and secondarily upregulates genes by activation of the IFNAR pathway. These pathways are crucial for driving the effector functions of NK cells and cytotoxic T cells that result in tumor regression after poly I:C treatment [6, 15].

NK cells are important for antitumor effects not only through direct cytotoxic activity, but also indirectly, through the production of cytokines including IFN-γ [16–20]. $DX5^+$ or $NK1.1^+$ cells have been used as conventional NK cells, which have features distinct from other lymphoid cells. Optimal NK cell responses require the presence of accessory cells such as DCs or macrophages [21]. NK cells are essential for poly I:C-induced growth retardation of NK-sensitive tumors such as B16 melanomas since poly I:C treatment does not induce antitumor activity in NK cell-depleted mice [4, 5]. IFN-γ production and cytotoxic activity by NK cells are potentiated by stimulating mice in vivo with poly I:C. NK cell activation appears to have many modes and myeloid NK cell contact serves a critical factor for antitumor NK cell activation.

Myeloid-derived suppressor cells (MDSCs) belongs to myeloid lineages with potent immunosuppressive activity against antitumor immune responses in mice and humans [22, 23]. MDSCs are widely distributed at tumor sites and in the peripheral organs, spleen and lymph nodes. Defined as a $CD11b^+Gr1^+$ subset in mice, they are heterogeneous populations of early myeloid progenitors that arise in bone marrow. Recently, they have also been found to originate from hematopoietic stem and progenitor cells accumulated in the spleen under tumor-bearing conditions [24]. The immunoregulatory functions of MDSCs in cancer have been studied extensively [22, 25]. MDSCs inhibit antigen-dependent T cell proliferation through the production of immunosuppressive factors including arginase-1, reactive oxygen species and reactive nitrogen species, and the release of immunosuppressive cytokines. However, the effect of MDSCs on NK cell function in tumor-bearing hosts is controversial. The anergy of NK cells is reportedly induced by MDSCs through membrane-bound TGF-β in a tumor-implant model using 3LL, B16 and EG7 cells [26]. MDSCs derived from patients with hepatocellular carcinoma inhibit autologous NK cell activity when cocultured in vitro [27]. Splenic MDSCs in TS/A tumor-bearing mice repress NK cell cytotoxicity [28]. A subset of MDSCs expresses NKG2D ligand on the cell surface and activates NK cells through NKG2D-NKG2D ligand interaction [29]. Although MDSCs express PRRs, their contribution to the MDSC function in poly I:C-induced growth retardation of tumors has not been fully understood.

Recent studies have demonstrated that TLR stimulation could modulate the function of immunosuppressive myeloid-derived cells as well as myeloid DCs in cancer. Tumor-associated macrophages and MDSCs were converted from tumor supporters to tumoricidal effectors after treatment with TLR agonists [7, 30, 31]. It was demonstrated that CpG treatment blocks MDSC-mediated T cell suppression associated with the maturation and differentiation of MDSCs [30, 31]. In this study, we revealed that poly I:C treatment allows cancer-expanded MDSCs to prime NK cells through the MAVS and the type-I IFN signaling pathway in vivo, leading to retardation of tumor growth.

Materials and Methods

Mice and Tumor Cells

Inbred C57BL/6 wild-type (WT) mice were purchased from Clea, Japan. $TICAM\text{-}1^{-/-}$ and $MAVS^{-/-}$ mice were generated in our laboratory. $IFNAR1^{-/-}$ mice were kindly provided by T. Taniguchi (University of Tokyo). Mice of 6- to 10-weeks of age were used in all experiments that were performed according to animal experimental ethics committee guidelines of Hokkaido University. B16D8 cells were developed in our laboratory [4]. B16D8 cells were cultured at 37°C under 5% CO_2 in RPMI containing 10% FBS, penicillin and streptomycin. This study was carried out in strict accordance with the recommendations in the Guide for the Care and Use of Laboratory Animals of the National Institutes of Health (USA). The protocol was approved by the Committee on the Ethics of Animal Experiments in the Animal Safety Center, Hokkaido University, Japan. All mice were used according to the guidelines of the institutional animal care and use committee of Hokkaido University, who approved this study as ID number 08-0290, 'Analysis of Anti-Tumor Immune Response Induced by the Activation of Innate Immunity'.

Tumor Challenge and Poly I:C Treatment

Mice were shaved at the back and injected s.c with B16D8 cells (6×10^5), 3LL cells (3×10^6) or EL4 cells (1×10^6) suspended in 200 μl PBS(−). Tumor size was measured using a caliper. Tumor volume was calculated using the following formula: tumor volume (cm^3) = (long diameter) × (short diameter)^2 × 0.4. Poly I:C (GE Bioscience) (200 μg/head) with no detectable LPS was injected i.p. as indicated. In some cases, polymixin B-treated poly I:C was used. When an average tumor volume of 0.4–0.6 cm^3 was reached, the treatment was started and was repeated every 4 days.

Cell Isolation and Culture

When tumor volume reached 1–2 cm^3, i.e. 14–18 days after tumor challenge, mice were injected i.p. with 200 μg poly I:C or PBS(–). After 4 h, $CD11b^+Gr1^+$ MDSC-like cells were isolated from splenocyte suspension or single-cell suspension from the collagenase-treated tumor of poly I:C-injected or PBS-injected mice by using biotin-conjugated anti-Gr1 monoclonal antibody (RB6–8C5) and Streptavidin Microbeads (Miltenyi) as described previously [7]. NK cells were purified from splenocytes of naïve mice by using DX5 Microbeads (Miltenyi). In these purification steps, two rounds of positive selection were performed. We routinely prepared $Gr1^+$ cells at more than 95% purity and almost 100% of $Gr1^+$ cells expressed CD11b. The purity of $DX5^+$ cells was more than 90%. Isolated $CD11b^+Gr1^+$ cells and $DX5^+$ cells were cocultured for 20–24 h. In some experiments, anti-IFNAR1 monoclonal antibody (MAR1–5A3) was added to the culture for neutralization of IFNAR1. Recombinant mouse IFN-α (R&D systems) was used for stimulation of $CD11b^+Gr1^+$ cells and NK cells.

Cells isolated from mouse spleen were incubated for 24 h and the conditioned medium was collected. Concentrations of IFN-α and IFN-γ were determined by ELISA according to manufacturer's instructions (PBL Interferon Source and eBioscience). NK cytotoxicity was determined by standard ^{51}Cr release assay as described previously [32].

Flow Cytometric Analysis

Mononuclear cells prepared from mouse spleen or tumor were treated with anti-CD16/32 (no. 93) and stained with FITC- or APC-anti-CD45.2 (no. 104), FITC- or PE-anti-CD11b (M1/70), APC- or PE-anti-GR1 (RB6–8C5), PE- or APC-anti-NK1.1 (PK136), PE-anti-CD49b (DX5), FITC-, PE- or APC-anti-CD3ε (145–2C11), FITC- or PE-anti-CD69 (H1.2F3), PE-anti-CD80 (16–10A1), PE-anti-CD86 (GL-1), PE-anti-CD40 (1C10), PE-anti-CD155 (TX56), PE-anti-CD70 (FR70), PE-anti-IL-15Ra (DNT15Ra), FITC-anti-CD150 [A12 (7D4)], and anti-RAE-1 (eBioscience and Biolegend). Samples were analyzed with a FACSCalibur instrument or FACS Aria instrument (BD Bioscience) and data analysis was performed by FlowJo software (Tree Star).

T Cell Proliferation Assay

T cell proliferation was measured by changes in fluorescence intensity using carboxyfluorescein diacetate succinimidyl ester (CFSE). Splenocytes from OT-I transgenic mice were labeled with 1 μM CFSE, placed into a round bottom 96-well plate containing $CD11b^+Gr1^+$ cells as indicated. Splenocytes were cultured in the presence of 100 nM OVA-derived peptide SIINFEKL. After 3 days, cells were harvested, stained with APC-anti-CD8α (53–6.7) and PE-anti-TCR vβ 5.1, 5.2 (MR9–4) or PE-anti-CD3ε (145–2C11), and the CFSE signal of gated lymphocytes was analyzed by flow cytometry. The extent of cell proliferation was quantified by FlowJo software (Tree Star).

Quantitative PCR Analysis

RNA was prepared with RNeasy kit (QIAGEN) or TRIZOL reagent (Invitrogen) according to the manufacturer's instruction. Reverse transcription was performed using High-Capacity cDNA Reverse Transcription kit (Applied Biosystems). Real-time PCR was performed with Power SYBR Green PCR Master Mix (Applied Biosystems) with StepOne™ Real-time PCR system (Applied Biosystems). Expression of the cytokine gene was normalized to the expression of glyceraldehyde phosphate dehydrogenase (GAPDH). The following primers were used for PCR: IFNα4 forward, 5′-CTGCTGGCTGTGAGGACATACT-3′, IFNα4 reverse, 5′-AGGCACAGAGGCTGTGTTTCTT-3′, IL-15 forward, 5′-TTAACTGAGGCTGGCATTCATG-3′, IL-15 reverse, 5′-ACCT ACACTGACACAGCCCAAA-3′, IL-18 forward, 5′-GACAAA GAAAGCCGCCTCAA-3′, IL-18 reverse, 5′-ATGGCAGCCAT TGTTCCTG-3′, INAM forward, 5′-CAACTGCAATGCCACG CTA-3′, INAM reverse, 5′-TCCAACCGAACACCTGAGACT-3′, GAPDH forward, 5′-GCCTGGAGAAACCTGCCA-3′, GAPDH reverse, 5′-CCCTCAGATGCCTGCTTCA-3′. Data was analyzed by the ΔΔCt method.

Statistics

If not otherwise stated, data were expressed as arithmetic means ± SD, and statistical analyses were made by 2-tailed Student's t test. $p < 0.05$ was considered statistically significant.

Results

$CD11b^+Gr1^+$ Cells Expanded in B16 Tumor-Bearing Mice Are Immunosuppressive

$CD11b^+Gr1^+$ cells representing MDSCs accumulate in large numbers in the lymphoid tissues of tumor-bearing mice [22, 23]. We therefore investigated the spleens of mice bearing syngenic tumor cells. B16 melanoma cells, 3LL lung cancer cells or EL4 thymoma cells were s.c. injected into WT mice and, 16 days later, splenic populations of immune cells were examined in the tumor-bearing mice. The proportion of $CD11b^+Gr1^+$ cells in the spleens of B16-implanted mice was higher than that in tumor-free naïve mice, consistent with previous reports (fig. 1a). Similar profiles were obtained with the 3LL and EL4 cell lines (data not shown).

To examine whether $CD11b^+Gr1^+$ cells had immunosuppressive activity, we harvested $CD11b^+Gr1^+$ cells from the spleens of B16 tumor-implanted mice, and cocultured $CD11b^+Gr1^+$ cells with OT-I splenocytes in the presence of OVA peptide. $CD11b^+Gr1^+$ cells from tumor-bearing mice efficiently inhibited antigen-specific proliferation of $CD8^+$ OT-I T cells (fig. 1b). Therefore, $CD11b^+Gr1^+$ cells accumulated in the spleen of B16 tumor-bearing mice and had immunosuppressive functions.

We also assessed the immunosuppressive activity of $CD11b^+Gr1^+$ cells against NK cells activated by PMA/ionomycin and tested activation as level of IFN-γ production. No inhibitory effect of $CD11b^+Gr1^+$ cells on the production of IFN-γ by NK cells was observed (online suppl. fig. 1; for all online suppl. material, see www.karger.com/doi/10.1159/000355126). Therefore, $CD11b^+Gr1^+$ cells expanded in B16 tumor-bearing mice exhibited immunosuppressive activity toward $CD8^+$ T cells but not NK cells.

In vivo Poly I:C Induces Cytokine Production and Maturation of CD11b⁺Gr1⁺ Cells

Type-I IFNs are systemically produced in tumor-bearing mice by i.p. injection of poly I:C. Poly I:C usually acts on TLR3 in myeloid/epithelial cells and MDA5 in systemic cells, leading to type-I IFN production [33]. Since CD11b⁺Gr1⁺ cells expressed both TLR3 and MDA5, we examined whether type-I IFNs were produced by CD11b⁺Gr1⁺ cells in B16 tumor-bearing mice in response to poly I:C injection. Interestingly, we found that IFN-α is produced in splenic CD11b⁺Gr1⁺ cells harvested from poly I:C-treated B16 tumor-bearing mice, but not in CD11b⁺Gr1⁺ cells unexposed to poly I:C (fig. 2a, left panel). The results were also confirmed in vitro: type-I IFNs was minimally produced in poly I:C-untreated CD11b⁺Gr1⁺ cells but robustly in poly I:C-treated cells from the spleen or tumor in direct response to poly I:C (fig. 2a, right panel). The results were reproducible with different tumor cell lines, specifically 3LL and EL4, and different sources of CD11b⁺Gr1⁺ cells

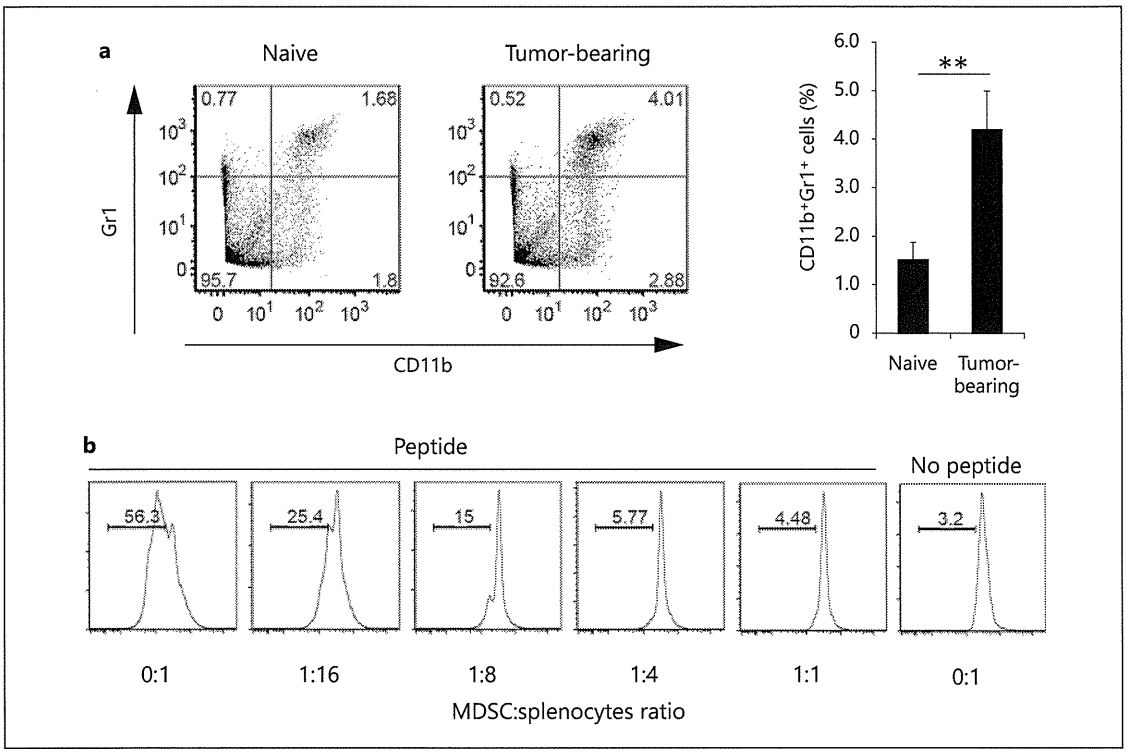

Fig. 1. Immunosuppressive activity of CD11b⁺Gr1⁺ cells in the spleen of B16 tumor-bearing mice. **a** WT mice were injected s.c. with B16D8 melanoma cells. The percentage of CD11b⁺Gr1⁺ cells in the spleen was determined on day 16 by flow cytometry (n = 6). Cells were gated on CD45⁺ cells. **b** CD11b⁺Gr1⁺ cells were isolated from spleens of B16 tumor-bearing mice, and cultured with CFSE-labeled OT-I splenocytes (1×10^6) at the indicated ratios. After 3 days, proliferation of CD8α⁺TCRvβ⁺ cells was measured. Data shown are representative of at least 2 independent experiments. ** $p < 0.01$.

Fig. 2. Effect of poly I:C treatment on CD11b⁺Gr1⁺ cells. **a** B16 tumor-bearing mice were injected i.p. with 200 μg poly I:C or PBS as a negative control. After 4 h, CD11b⁺Gr1⁺ cells were purified from spleens and incubated for 24 h (left panel). CD11b⁺Gr1⁺ cells isolated from spleens of B16 tumor-bearing mice were treated with 50 μg/ml poly I:C or PBS for 24 h (right panel). The concentration of IFN-α in conditioned medium was determined. **b** 3LL cells (3×10^6) were implanted into B6 WT mice and CD11b⁺Gr1⁺ cells were isolated from spleen (left panel) or tumor (right panel) after poly I:C injection as described in **a**. **c** Spleen cells were prepared from B16 tumor-bearing mice treated with poly I:C or PBS for 8 h as described in **a** and surface expression of CD80, CD86, CD40, RAE-1, CD155, CD70, IL-15RA and CD150 on CD11b⁺Gr1⁺ cells was determined. **d** CD11b⁺Gr1⁺ cells were isolated from B16 tumor-bearing mice treated with poly I:C or PBS for 4 h as described in **a** and mRNA for IFN-α4, IL-15, IL-18, INAM and arginase-1 was measured (n = 3). Data shown are representative of at least 2 independent experiments. ** $p < 0.01$, * $p < 0.05$. NS = Not significant.

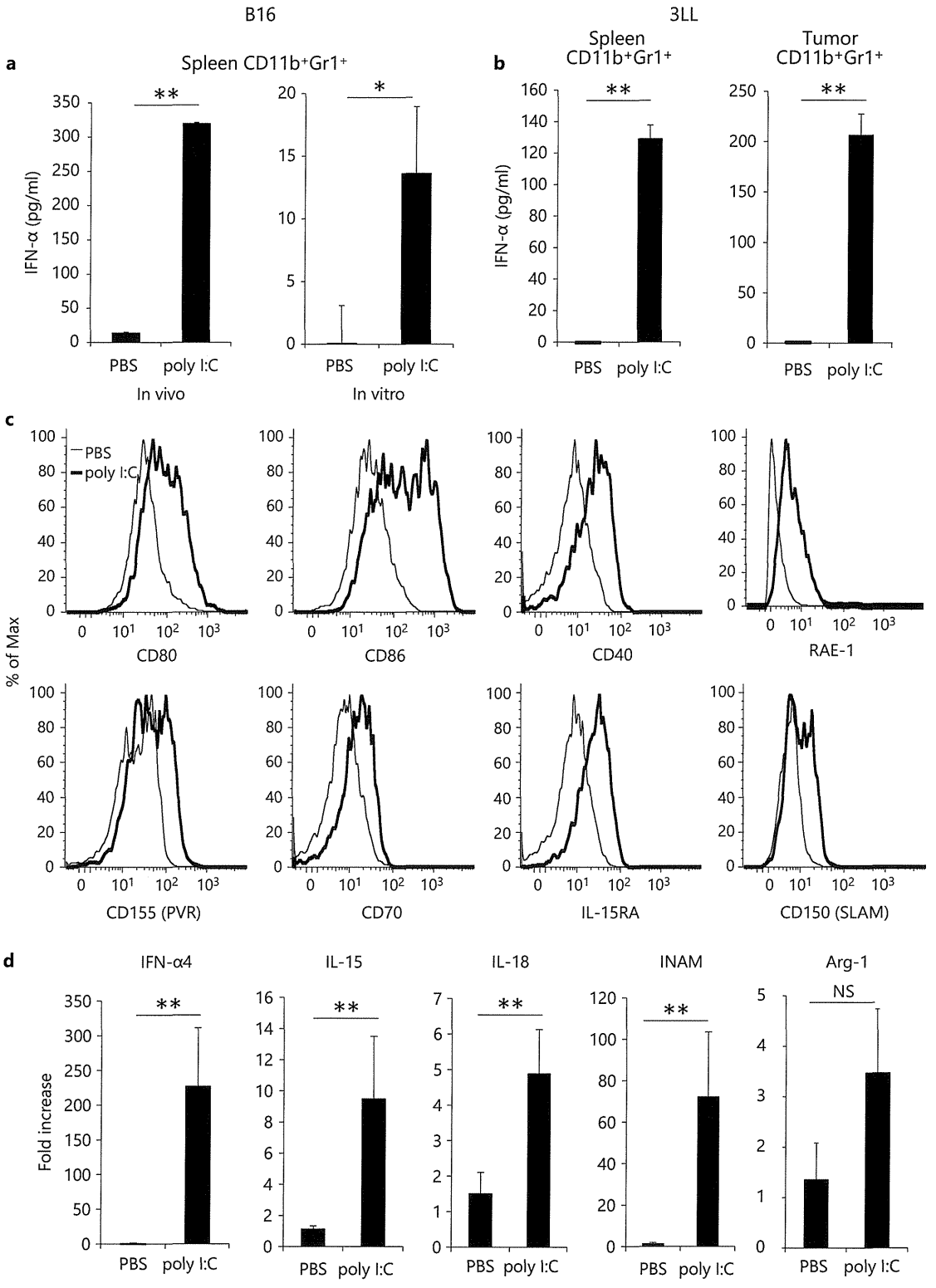

2

(fig. 2b; online suppl. fig. 2a). In addition, the costimulatory molecules CD80 and CD86 on these cells were upregulated in response to poly I:C (fig. 2c). To further investigate the effect of poly I:C treatment on the function of $CD11b^+Gr1^+$ cells, we analyzed the gene expression of $CD11b^+Gr1^+$ cells isolated from B16 tumor-bearing mice, 4 h after injection with poly I:C or PBS. We found an increase in mRNA for IFN-α4, IL-15, IL-18 and INAM (fig. 2d) [21, 32]. Furthermore, in vivo poly I:C treatment for 8 h resulted in upregulation of RAE-1, PVR (CD155), CD70, IL-15RA, SLAM (CD150) and CD40 on $CD11b^+Gr1^+$ cell surface (fig. 2c). These molecules are involved in DC-mediated NK cell activation [18, 34, 35]. However, mRNA for arginase-1, which is involved in MDSC-mediated inhibition of T cell proliferation, was not increased in $CD11b^+Gr1^+$ cells (fig. 2d). These results suggest that in vivo pretreatment of mice with poly I:C effectively induces the maturation of $CD11b^+Gr1^+$ cells, resulting in enhanced expression of NK cell-activating molecules.

$CD11b^+Gr1^+$ Cells from Poly I:C-Treated Tumor-Bearing Mice Activate NK Cells

To investigate whether $CD11b^+Gr1^+$ cells from poly I:C-injected tumor-bearing mice are capable of activating NK cells, we isolated $CD11b^+Gr1^+$ cells from the spleens of tumor-bearing mice after poly I:C administration and cocultured the cells with NK cells from naïve mice. NK cells upregulated CD69 on their surface in response to the $CD11b^+Gr1^+$ cells from poly I:C-injected B16 tumor-bearing mice. However, the level of CD69 on NK cells was not changed when the cells were mixed with $CD11b^+Gr1^+$ cells from PBS-injected tumor-bearing mice (fig. 3a, left panel). $CD11b^+Gr1^+$ cells from poly I:C-injected tumor-bearing mice also induced NK cell IFN-γ production (fig. 3a, right panel). Similar results were obtained with NK cells cocultured with $CD11b^+Gr1^+$ cells from mice bearing 3LL- or EL4 cell tumors after poly I:C treatment (fig. 3b, c; online suppl. fig. 2b, c). Furthermore, $CD11b^+Gr1^+$ cells from tumors of 3LL-implant mice had a similar ability to induce IFN-γ production and CD69 expression in NK cells after poly I:C treatment (fig. 3c). IFN-γ inhibits proliferation of B16 cells in vitro without affecting the cell viability (online suppl. fig. 3; data not shown). In contrast, $CD11b^+Gr1^+$ cells did not drive a cytotoxic phenotype from NK cells (fig. 3d). In vitro stimulation of $CD11b^+Gr1^+$ cells with poly I:C did not induce NK cytotoxicity in coculture (data not shown). These results demonstrated that when poly I:C was injected into tumor-bearing mice, $CD11b^+Gr1^+$ cells acquired the ability to prime NK cells as measured by CD69 expression and IFN-γ production, but did not induce cytotoxic activity.

Type-I IFN Signaling Is Essential for NK Cell Priming by $CD11b^+Gr1^+$ Cells

Next, we investigated the mechanisms by which $CD11b^+Gr1^+$ cells primed NK cells through the in vivo administration of poly I:C. Soluble factors and membrane-associated molecules induced by poly I:C are reportedly involved in in vivo NK cell activation [15, 18]. As shown in figure 2a, $CD11b^+Gr1^+$ cells from poly I:C-treated tumor-bearing mice produced IFN-α. To examine whether type-I IFN signaling through IFNAR was involved in NK cell activation, we added anti-IFNAR1 antibodies to cultures to inhibit type-I IFN signaling by both $CD11b^+Gr1^+$ and NK cells that express IFNAR1. CD69 upregulation on NK cells and IFN-γ production induced by activated $CD11b^+Gr1^+$ cells were completely abrogated by anti-IFNAR1 antibodies (fig. 4a). These results suggest that type-I IFN signaling is essential for NK cell priming by $CD11b^+Gr1^+$ cells.

To investigate type-I IFN signaling in NK cell priming, we prepared NK cells from $IFNAR1^{-/-}$ mice. $IFNAR1^{-/-}$ NK cells were cocultured with $CD11b^+Gr1^+$ cells. $CD11b^+Gr1^+$ cells from poly I:C-stimulated WT mice stimulated CD69 expression and IFN-γ production by WT NK cells but not $IFNAR1^{-/-}$ NK cells (fig. 4b). Therefore, type-I IFN signaling in NK cells is essential for NK priming by $CD11b^+Gr1^+$ cells.

To examine whether IFNAR signaling is the only route for the induction of $CD11b^+Gr1^+$ cell-mediated NK priming, we added recombinant mouse IFN-α to cultures of NK cells or to cocultures of untreated $CD11b^+Gr1^+$ cells and WT NK cells. Recombinant mouse IFN-α in NK cell cultures resulted in induction of CD69 expression on the NK cells (fig. 4c, left panels). However, CD69 expression was minimally augmented in the NK cells cocultured with $CD11b^+Gr1^+$ cells. In contrast, NK cell IFN-γ production was clearly induced at high concentrations of IFN-α (2,000 IU/ml) and augmented by $CD11b^+Gr1^+$ cells (fig. 4c, right panel).

We investigated if cell-cell contact is involved in NK cell activation in cocultures of $CD11b^+Gr1^+$ cells and naïve NK cells using the Transwell system. Sufficient NK cell priming was detected when NK cells were cocultured with in vivo poly I:C-activated $CD11b^+Gr1^+$ cells. However, expression of CD69 and production of IFN-γ by NK cells was abrogated by separation of the cells by the Transwell membrane (online suppl. fig. 4a, b). These results,

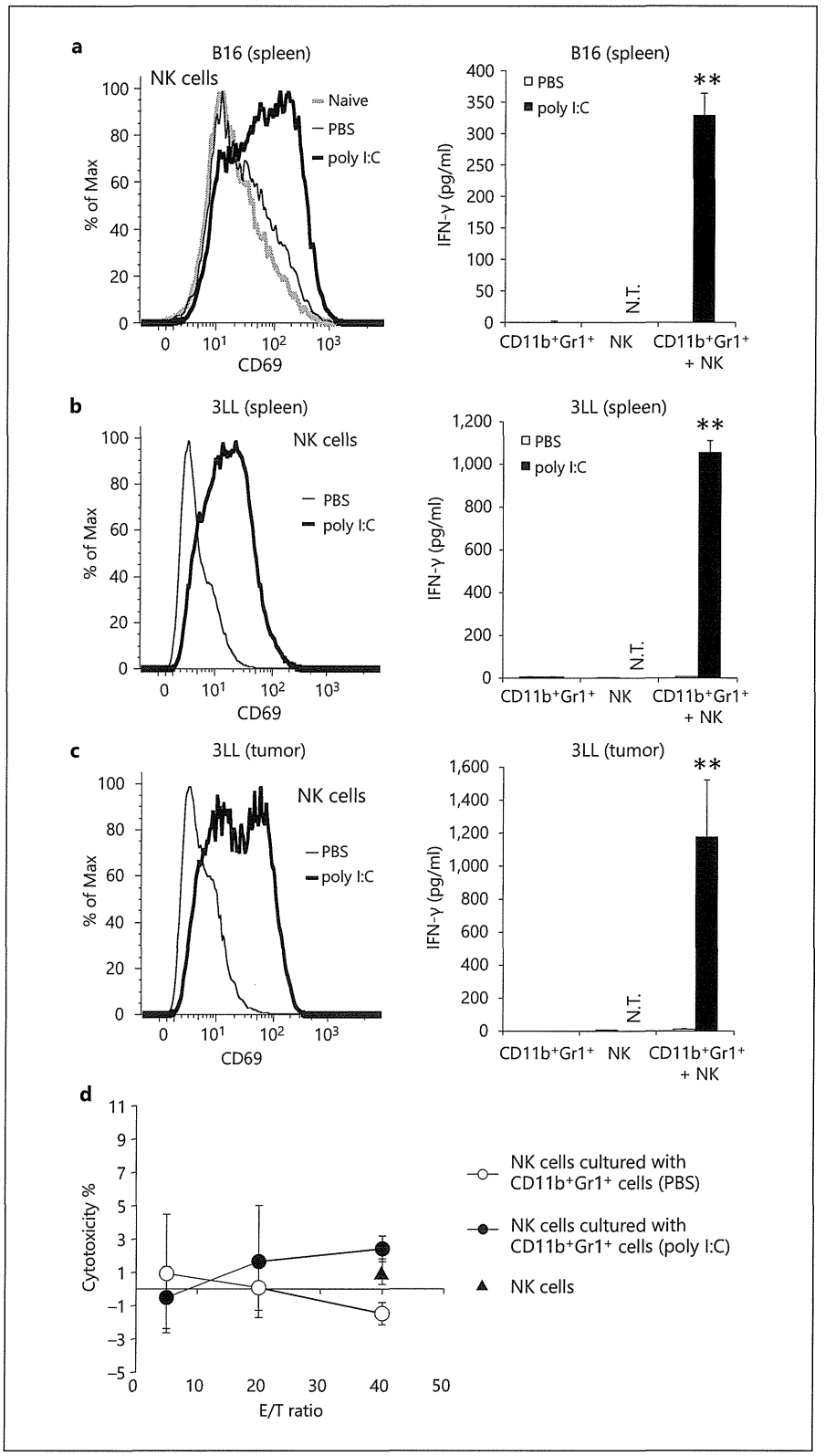

Fig. 3. NK cells are primed by $CD11b^+Gr1^+$ cells isolated from poly I:C-injected tumor-bearing mice. **a–c** $CD11b^+Gr1^+$ cells were isolated from spleens or tumors of B16 (**a**), 3LL (**b**, **c**) tumor-bearing mice pretreated with 200 μg poly I:C or PBS for 4 h and cultured with NK cells from naïve WT mice. After 24 h, CD69 expression on NK cells (**a–c**, left panels) and IFN-γ concentration in conditioned medium (**a–c**, right panels) were determined. CD69 expression of $NK1.1^+CD3\varepsilon^-$ cells is indicated (**a–c**). N.T. = Not tested. **d** Cytotoxic activity of NK cells cocultured with or without $CD11b^+Gr1^+$ cells isolated from poly I:C- or PBS-treated tumor-bearing mice was determined by standard ^{51}Cr release assay (n = 3). Triangle: NK cells not cultured with $CD11b^+Gr1^+$ cells. Data shown are representative of at least 3 independent experiments. ** $p < 0.01$.

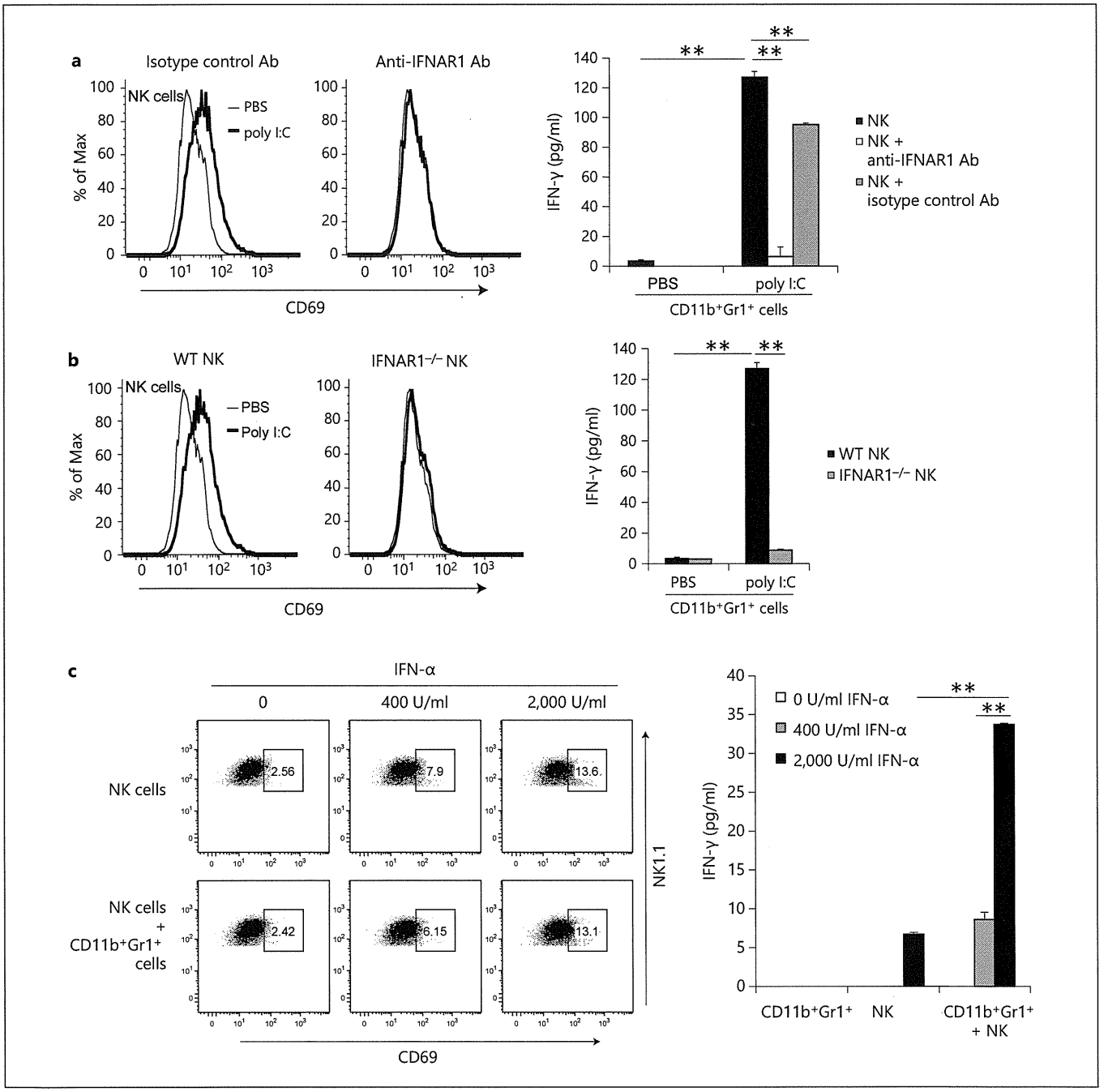

Fig. 4. Type-I IFNs from CD11b$^+$Gr1$^+$ cells and IFNAR in NK cells are indispensable for NK cell activation. **a** CD11b$^+$Gr1$^+$ cells were isolated from spleens of B16 tumor-bearing mice treated with 200 μg poly I:C or PBS for 4 h and cultured with NK cells from naïve WT mice in the presence or absence of 10 μg/ml anti-IFNAR1 antibody (Ab). After 24 h, CD69 expression on NK cells (left panels) and IFN-γ concentration in conditioned medium (right panel) was determined (n = 3). **b** CD11b$^+$Gr1$^+$ cells isolated as described in **a** were cultured for 24 h with NK cells from naïve WT mice or IFNAR1$^{-/-}$ mice, and CD69 expression (left panels) and IFN-γ production were measured (n = 3) (right panel). **c** Recombinant IFN-α was added to cultures of naïve NK cells with or without CD11b$^+$Gr1$^+$ cells from nontreated tumor-bearing mice. After incubation for 24 h, CD69 expression on NK cells (left panels) and IFN-γ concentration in conditioned medium (right panel) were determined (n = 3). CD69 expression of NK1.1$^+$CD3ε$^-$ cells is indicated (**a–c**). Data shown are representative of two independent experiments. ** $p < 0.01$.

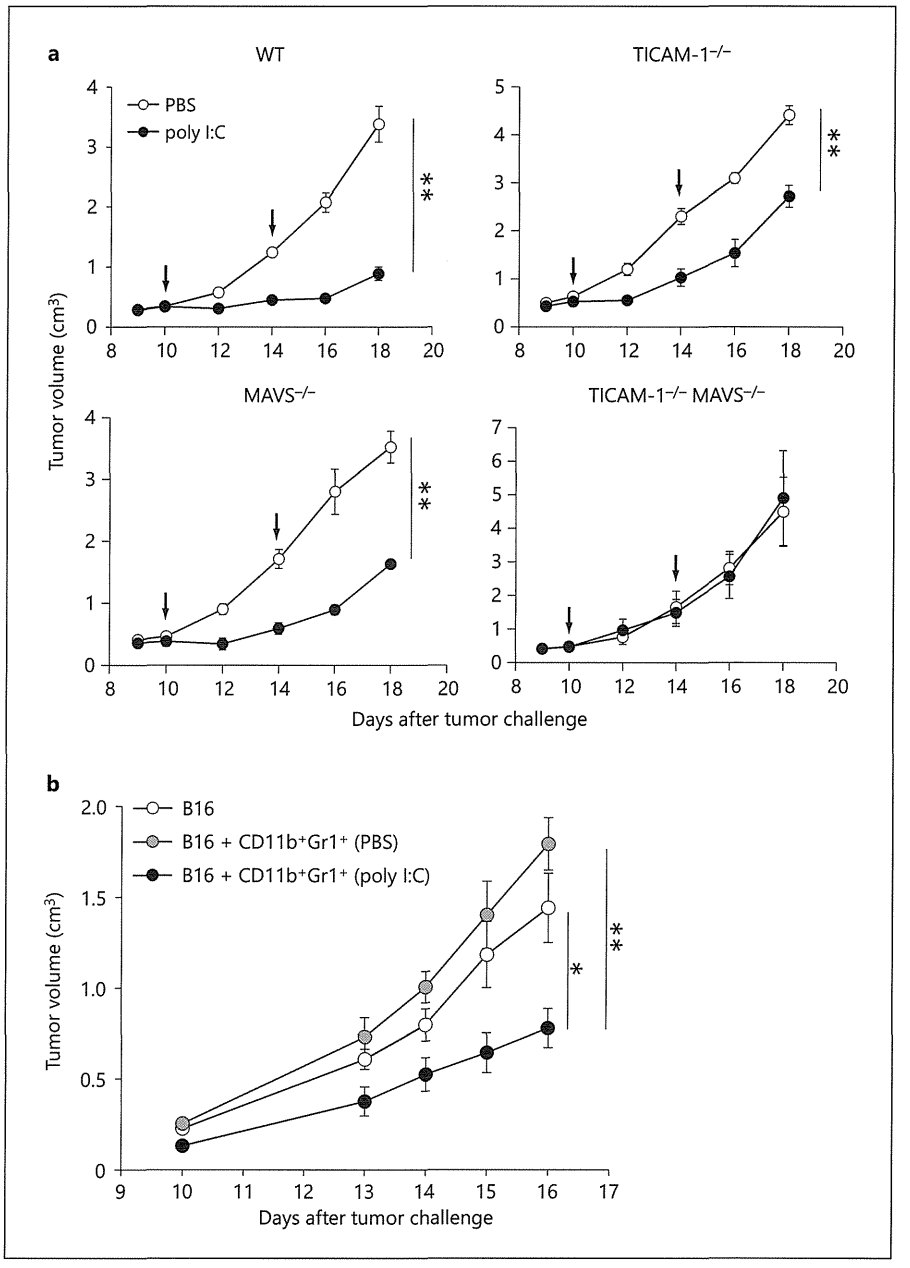

Fig. 5. Retardation of B16 tumor growth by poly I:C treatment in mouse models. **a** Both TICAM-1 and MAVS signals are involved in B16 tumor growth retardation after poly I:C therapy. B16 cells (6×10^5) were implanted s.c. into WT, TICAM-$1^{-/-}$, MAVS$^{-/-}$ and TICAM-1 and MAVS double-knockout mice. Tumor-bearing mice were treated with 200 μg poly I:C or PBS on days 10 and 14 (arrows) (n = 3–5 per group). Data are average ± SEM. **b** In vivo poly I:C-activated CD11b$^+$Gr1$^+$ cells inhibit B16 tumor growth. B16 cells (6×10^5) were mixed with or without CD11b$^+$Gr1$^+$ cells (1×10^6) from spleens of B16 tumor-bearing mice treated with 200 μg poly I:C or PBS for 4 h. Cell mixtures were implanted s.c. into WT mice on day 0 (n = 4 per group). Data are average ± SEM and are representative of 2 independent experiments. ** $p < 0.01$, * $p < 0.05$.

together with the results in figure 4, suggest that two modes of NK priming occur simultaneously in CD11b$^+$Gr1$^+$ cells: one mode is through type-I IFN production and the other is via cell-cell contact.

MAVS and IFNAR Are Required to Activate MDSCs with in vivo Poly I:C Treatment

Poly I:C induces growth retardation of B16 tumors implanted in WT mice [4–6, 36]. To determine the signaling pathway that is essential for the retardation of B16 tumor growth in vivo, we implanted B16 melanoma cells s.c. into TICAM-$1^{-/-}$ and MAVS$^{-/-}$ mice. B16 tumor growth was monitored after poly I:C injection. Marked tumor growth retardation was observed in poly I:C-treated mice (fig. 5a). The poly I:C antitumor effect was only partly abrogated in either TICAM-$1^{-/-}$ or MAVS$^{-/-}$ mice and was completely abolished in TICAM-$1^{-/-}$/MAVS$^{-/-}$ mice (fig. 5a). Therefore, both TICAM-1 and MAVS signals are involved in the antitumor activity of poly I:C, consistent with earlier reports [4, 5, 33].

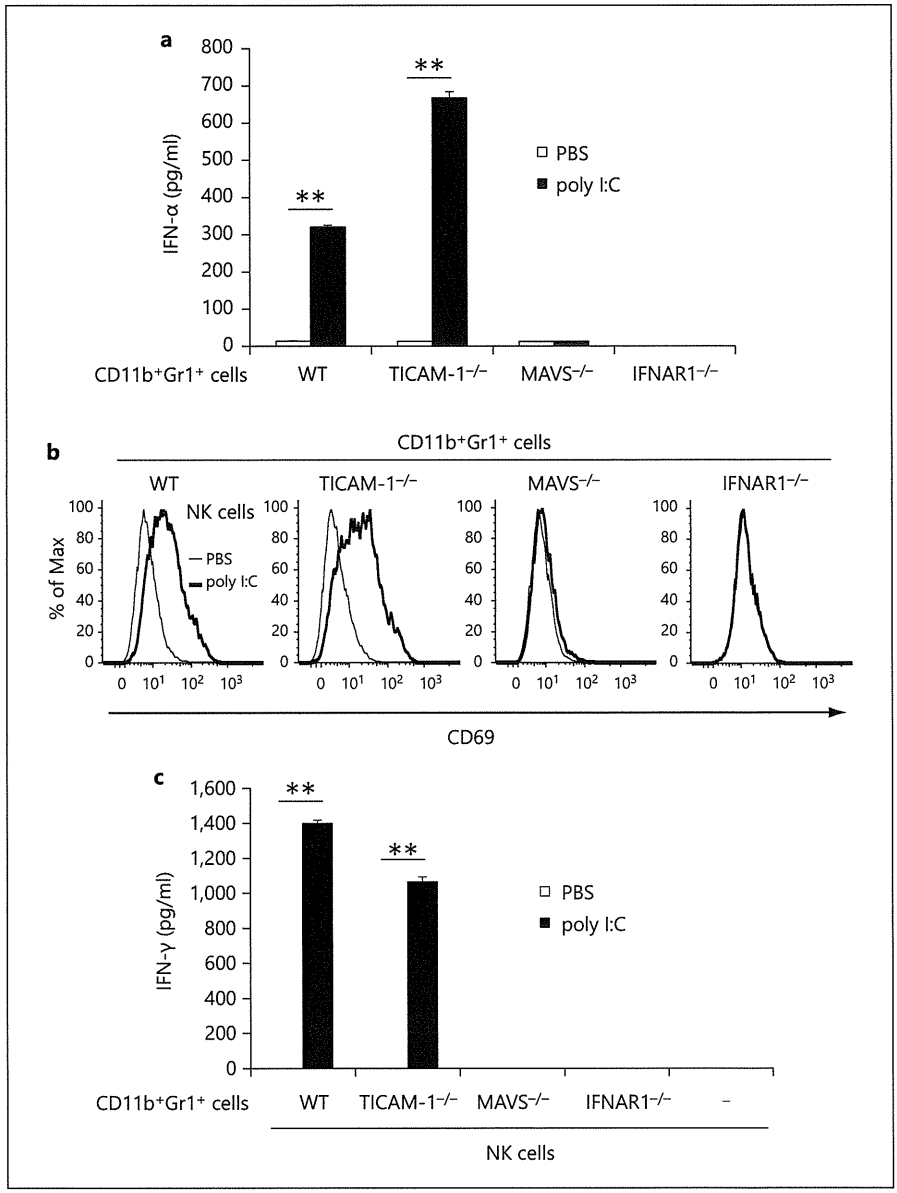

Fig. 6. MAVS and type-I IFN signaling pathways are critical for CD11b$^+$Gr1$^+$ cell activation in vivo. **a** B16 cells (6×10^5) were implanted into WT, TICAM-1$^{-/-}$, MAVS$^{-/-}$ or IFNAR1$^{-/-}$ mice. Tumor-bearing mice were treated with 200 μg poly I:C or PBS for 4 h and CD11b$^+$Gr1$^+$ cells were isolated from spleens, and allowed to stand for 24 h. IFN-α concentration in conditioned medium was determined (n = 3). **b**, **c** CD11b$^+$Gr1$^+$ cells were isolated from KO mouse lines as described in **a**, and were cultured with naïve WT NK cells for 24 h. CD69 expression on NK cells (**b**) and IFN-γ concentration in conditioned medium (**c**) were determined (n = 3). Data shown are representative of 3 independent experiments. ** $p < 0.01$.

Next, we determined the mechanisms involved in the in vivo activation of CD11b$^+$Gr1$^+$ cells by poly I:C. To investigate the signaling pathway that was important for poly I:C-induced activation of CD11b$^+$Gr1$^+$ cells in vivo, we challenged TICAM-1$^{-/-}$ and MAVS$^{-/-}$ mice with B16 melanoma cells. After tumor formation, poly I:C was injected i.p. into the mice and CD11b$^+$Gr1$^+$ cells were isolated from the spleen and were cocultured with naïve WT NK cells. CD11b$^+$Gr1$^+$ cells from tumor-bearing TICAM-1$^{-/-}$ mice produced IFN-α at levels comparable to cells from WT mice (fig. 6a). In parallel, CD69 expression on NK cells and IFN-γ production was observed in conditioned medium from mixed cultures of TICAM-1$^{-/-}$ CD11b$^+$Gr1$^+$ cells and naïve WT NK cells. The results suggest that in vivo TICAM-1 signaling is not mandatory for CD11b$^+$Gr1$^+$ cell activation to induce NK cell priming (fig. 6a–c). CD11b$^+$Gr1$^+$ cells from tumor-bearing MAVS$^{-/-}$ mice treated with poly I:C did not produce IFN-α or induce CD69 expression and IFN-γ production in NK cells (fig. 6a–c). Similar results were obtained with CD11b$^+$Gr1$^+$ cells from B16 tumor-bearing IFNAR1$^{-/-}$ mice (fig. 6a–c). These results suggest that MAVS as well as type-I IFN signaling is crucial for poly I:C-dependent NK cell priming in CD11b$^+$Gr1$^+$ cells of tumor-bearing mice.

The MAVS pathway is conserved in most cell types in mice. We examined whether NK cell priming induced by poly I:C (i.e. MAVS signal)-activated $CD11b^+Gr1^+$ cells was involved in retardation of B16 tumor growth. NK-sensitive B16 tumor cells were mixed with $CD11b^+Gr1^+$ cells isolated from poly I:C (or control PBS)-injected tumor-bearing mice, and inoculated s.c. into WT mice (fig. 5b). Significant B16 growth retardation was detected only in those tumors containing poly I:C-treated $CD11b^+Gr1^+$ cells (fig. 5b). The B16 tumors with intact $CD11b^+Gr1^+$ cells showed higher growth rates than B16 tumor cells only, which might reflect the previously-reported tumor-supporting activity of MDSCs [37]. Thus, MDSC-like $CD11b^+Gr1^+$ cells can be converted to cells with an NK-priming activity that induces growth retardation of NK-sensitive tumors in mice. NK-priming would be a condition prior to full activation of antitumor NK cells.

Discussion

We demonstrated that in vivo poly I:C treatment led to $CD11b^+Gr1^+$ MDSC maturation and cytokine production in tumor-bearing mice. Poly I:C treatment rendered tumor and spleen MDSCs competent for $DX5^+$ NK cell priming as measured by CD69 expression and IFN-γ production. Poly I:C-dependent NK priming raises through the MAVS pathway (fig. 6). Among a number of proteins that were upregulated after poly I:C treatment, type-I IFN produced by activated MDSCs was critical for NK cell priming since it activated the IFNAR pathway in NK cells. However, NK cells barely exerted direct cytotoxic activity to B16 cells in response to poly I:C-matured MDSCs. This NK activation profile resembles that of IFN-γ-producing innate lymphoid cells. Some populations of these innate lymphocytes produce IFN-γ but exhibit little cytotoxic activity [38], similar to the NK cells affected by MDSC. These findings would allow us to speculate that the production of IFN-γ without cytotoxic activity is an activation state of NK cells or innate lymphocytes where MDSCs contribute.

In tumor-bearing hosts, poly I:C treatment resulted in tumor regression. Poly I:C induces direct killing of 3LL tumor cells by M2-M1 conversion of tumor-associated macrophages [7]. The TICAM-1 signal facilitates tumor-associated macrophage conversion as well as cross-presentation by DCs leading to antigen-specific CTL induction, which is also evoked by poly I:C [8]. The action of $CD11b^+Gr1^+$ MDSCs on implant B16 tumor was tumor-supporting when MDSCs were embedded into the tumor (fig. 5b). However, once MDSCs were pretreated with poly I:C and mixed with B16 cells, tumor growth was prohibited (fig. 5b). The result suggests that MDSC has plasticity to change the function from tumor-supporting to tumor-suppressing even in vivo. Here, we highlight the first evidence of MDSCs to evoke NK cell priming, which ultimately associates with retardation of tumor growth.

Although the exact mechanism of tumor regression by MDSC-NK activation remains to be elucidated, we speculate that IFN-γ produced by the primed NK cells could evoke antitumor activity. One possibility is that IFN-γ directly inhibits the growth of a certain tumor line including B16 melanoma by inducing cell cycle arrest. IFN-γ has a synergistic effect on type-I IFNs, arresting cell cycle to cell death in some tumor cell lines independent of p53 [39]. IFN-γ also induces angiostasis, which prevents rapid tumor progression [19], and inhibits metastasis and proliferation of B16 melanoma [17, 20]. In fact, we observed that IFN-γ directly inhibits proliferation of B16 cells in vitro, suggesting that NK cell-derived IFN-γ might inhibit B16 tumor growth during poly I:C treatment (online suppl. fig. 3).

Retardation of B16 growth was partially abrogated in TICAM-$1^{-/-}$ or $MAVS^{-/-}$ mice and completely abrogated in TICAM-$1^{-/-}$, $MAVS^{-/-}$ double KO mice (fig. 5a), the two pathways contributing to in vivo poly I:C-derived tumor suppression. In addition, MDSC activation is completely abrogated in $IFNAR1^{-/-}$ mice and IFNAR in NK cells is involved in efficient IFN-γ production induced by activated MDSCs. Type-I IFN receptor signaling is crucial for growth retardation of B16 tumor in poly I:C therapy. Therefore, a variety of situations result in NK activation/priming in the therapeutic use of poly I:C in tumor-bearing mice, although IFNAR is the common factor.

Miyake et al. [5], reported that MAVS is responsible for NK cell-dependent tumor regression using $MAVS^{-/-}$ mice with poly I:C stimulation ; however, the cell types for the poly I:C response and the mechanism of induction of NK-sensitive tumor regression remain undefined. NK-activating ligands on the DC surface as well as soluble factors induced by IRF-3 and IFNAR stimulation are crucial for DC-mediated NK cell activation [15, 32]. In addition, MDSC is a cell type that specifically drives NK priming through the MAVS pathway (fig. 6). MAVS-dependent IRF-3 activation occurs through stromal cells other than DCs, and these cells including MDSCs participate in NK-sensitive tumor regression. The result of this MDSC function is in contrast to that of DCs where the TLR3/TICAM-1 pathway preferentially promotes NK cell acti-

vation [4]. Specific depletion of MDSCs in preformed tumors, if possible, would enable us to confirm the functional importance of MAVS in tumor regression reported by Miyake et al. [5], who postulated that stromal cells were a source of the cell type that induces MAVS-mediated NK priming. However, the function of poly I:C via the MDSC-NK cell pathway is only a part of the total antitumor activity of poly I:C, which would be difficult to detect by tumor-size reduction. MDSCs are expanded in a late phase of implant tumor, where poly I:C may act on MDSCs and exert antitumor activity via poly I:C-stimulated MDSCs.

A recent report suggested that type-I IFNs act on accessory cells such as DCs, leading to the production of IL-15, IL-12, IL-18 and NKG2D ligands such as RAE-1. IFN-α acted on NK cells and slightly induced IFN-γ production, which was augmented in the presence of MDSCs. Cell-cell interaction between MDSCs and NK cells appears to be required for robust IFN-γ production. Induction of NK-activating ligands in association with natural NK cytotoxicity is involved in cell-cell contact-mediated NK cell activation. We found mRNA for downstream genes of IRF-3, especially IL-15, IL-18, INAM and RAE-1 elevated in MDSCs after treatment with poly I:C. However, IL-15 and RAE-1 appear not to participate in IFN-γ production by NK cells with MDSCs because neutralizing antibodies to IL-15, RAE-1 or NKG2D did not inhibit IFN-γ production by NK cells. Therefore, other molecules should be involved in NK cell activation by MDSCs. In fact, INAM or other molecules expressed on the MDSC surface sustain NK cell activation following poly I:C treatment (fig. 2; data not shown) as in bone marrow-derived cells [32].

MDSCs that have expanded in tumor-bearing hosts strongly suppress antitumor immune responses [22, 23]. Reduction of MDSC population or function is achieved by treatment with reagents that are related to improvement in tumor-specific immunity [40]. Furthermore, maturation of MDSCs can be accomplished through IFN-α production by plasmacytoid DCs or direct TLR9 stimulation, which contributes to tumor regression [30, 31]. Direct administration of IFN-α, i.e. IFN therapy, however, has not been successful as a universal therapy in cancer patients. Serious side effects are associated with high therapeutic doses of type-I IFN as well as poly I:C. Development of less toxic reagents with sufficient IRF-3/7 activation would be important for anti-MDSC cancer therapy.

Acknowledgements

We thank Drs. H. Takaki, J. Kasamatsu, K. Funami, M. Tatematsu and M. Azuma in our laboratory for their fruitful discussions. This work was supported in part by Grants-in-Aids from the Ministry of Education, Science and Culture (specified project for advanced research) and the Ministry of Health, Labor and Welfare of Japan as well as by the Akiyama Life Science Foundation (H.S.), the Takeda Science Foundation (H.S.), the Yasuda Cancer Foundation (T.S.) and the Ono Foundation (T.S.). Financial support by a MEXT Grant-in-Project 'the Carcinogenic Spiral', 'the National Cancer Center Research and Development Fund (23-A-44)', and the Japan Initiative for Global Research Network on Infectious Diseases is gratefully acknowledged.

References

1 Galluzzi L, Vacchelli E, Eggermont A, Fridman WH, Galon J, Sautès-Fridman C, et al: Trial watch: experimental Toll-like receptor agonists for cancer therapy. Oncoimmunol 2012;1:699–716.
2 Desmet CJ, Ishii KJ: Nucleic acid sensing at the interface between innate and adaptive immunity in vaccination. Nat Rev Immunol 2012;12:479–491.
3 Seya T, Shime H, Ebihara T, Oshiumi H, Matsumoto M: Pattern recognition receptors of innate immunity and their application to tumor immunotherapy. Cancer Sci 2010;101:313–320.
4 Akazawa T, Ebihara T, Okuno M, Okuda Y, Shingai M, Tsujimura K, et al: Antitumor NK activation induced by the Toll-like receptor 3-TICAM-1 (TRIF) pathway in myeloid dendritic cells. Proc Natl Acad Sci USA 2007;104:252–257.
5 Miyake T, Kumagai Y, Kato H, Guo Z, Matsushita K, Satoh T, et al: Poly I:C-induced activation of NK cells by CD8 alpha+ dendritic cells via the IPS-1 and TRIF-dependent pathways. J Immunol 2009;183:2522–2528.
6 Salem ML, El-Naggar SA, Kadima A, Gillanders WE, Cole DJ: The adjuvant effects of the Toll-like receptor 3 ligand polyinosinic-cytidylic acid poly (I:C) on antigen-specific CD8+ T cell responses are partially dependent on NK cells with the induction of a beneficial cytokine milieu. Vaccine 2006;24:5119–5132.
7 Shime H, Matsumoto M, Oshiumi H, Tanaka S, Nakane A, Iwakura Y, et al: Toll-like receptor 3 signaling converts tumor-supporting myeloid cells to tumoricidal effectors. Proc Natl Acad Sci USA 2012;109:2066–2071.
8 Azuma M, Ebihara T, Oshiumi H, Matsumoto M, Seya T: Cross-priming for antitumor CTL induced by soluble Ag + poly I:C depends on the TICAM-1 pathway in mouse CD11c+/CD8α+ dendritic cells. Oncoimmunol 2012;1:581–592.
9 Gauzzi MC, Del Corno M, Gessani S: Dissecting TLR3 signalling in dendritic cells. Immunobiology 2010;215:713–723.
10 Oshiumi H, Matsumoto M, Funami K, Akazawa T, Seya T: TICAM-1, an adaptor molecule that participates in Toll-like receptor 3-mediated interferon-β induction. Nat Immunol 2003;4:161–167.
11 Yamamoto M, Sato S, Hemmi H, Hoshino K, Kaisho T, Sanjo H, et al: Role of adaptor TRIF in the MyD88-independent Toll-like receptor signaling pathway. Science 2003;301:640–643.
12 Seth RB, Sun L, Ea C-K, Chen ZJ: Identification and characterization of MAVS, a mitochondrial antiviral signaling protein that activates NF-κB and IRF3. Cell 2005;122:669–682.

13 Honda K, Takaoka A, Taniguchi T: Type I inteferon gene induction by the interferon regulatory factor family of transcription factors. Immunity 2006;25:349–360.
14 Kawai T, Sato S, Ishii KJ, Coban C, Hemmi H, Yamamoto M, et al: Interferon-alpha induction through Toll-like receptors involves a direct interaction of IRF7 with MyD88 and TRAF6. Nat Immunol 2004;5:1061–1068.
15 Seya T, Kasamatsu J, Azuma M, Shime H, Matsumoto M: Natural killer cell activation secondary to innate pattern sensing. J Innate Immun 2011;3:264–273.
16 Zamai L, Ponti C, Mirandola P, Gobbi G, Papa S, Galeotti L, et al: NK cells and cancer. J Immunol 2007;178:4011–4016.
17 Takeda K, Nakayama M, Sakaki M, Hayakawa Y, Imawari M, Ogasawara K, et al: IFN-γ production by lung NK cells is critical for the natural resistance to pulmonary metastasis of B16 melanoma in mice. J Leukoc Biol 2011;90:777–785.
18 Vivier E, Tomasello E, Baratin M, Walzer T, Ugolini S: Functions of natural killer cells. Nat Immunol 2008;9:503–510.
19 Hayakawa Y, Takeda K, Yagita H, Smyth MJ, Van Kaer L, Okumura K, et al: IFN-γ-mediated inhibition of tumor angiogenesis by natural killer T-cell ligand, α-galactosylceramide. Blood 2002;100:1728–1733.
20 Kakuta S, Tagawa Y-I, Shibata S, Nanno M, Iwakura Y: Inhibition of B16 melanoma experimental metastasis by interferon-gamma through direct inhibition of cell proliferation and activation of antitumour host mechanisms. Immunology 2002;105:92–100.
21 Newman K, Riley E: Whatever turns you on: accessory-cell-dependent activation of NK cells by pathogens. Nat Rev Immunol 2007;7:279–291.
22 Gabrilovich DI, Ostrand-Rosenberg S, Bronte V: Coordinated regulation of myeloid cells by tumours. Nat Rev Immunol 2012;12:253–268.
23 Ostrand-Rosenberg S, Sinha P: Myeloid-derived suppressor cells: linking inflammation and cancer. J Immunol 2009;182:4499–4506.
24 Cortez-Retamozo V, Etzrodt M, Newton A, Rauch PJ, Chudnovskiy A, Berger C, et al: Origins of tumor-associated macrophages and neutrophils. Proc Natl Acad Sci USA 2012;109:2491–2496.
25 Ostrand-Rosenberg S: Myeloid-derived suppressor cells: more mechanisms for inhibiting antitumor immunity. Cancer Immunol Immunother 2010;59:1593–1600.
26 Li H, Han Y, Guo Q, Zhang M, Cao X: Cancer-expanded myeloid-derived suppressor cells induce anergy of NK cells through membrane-bound TGF-β1. J Immunol 2009;182:240–249.
27 Hoechst B, Voigtlaender T, Ormandy L, Gamrekelashvili J, Zhao F, Wedemeyer H, et al: Myeloid derived suppressor cells inhibit natural killer cells in patients with hepatocellular carcinoma via the NKp30 receptor. Hepatology 2009;50:799–807.
28 Liu C, Yu S, Kappes J, Wang J, Grizzle WE, Zinn KR, et al: Expansion of spleen myeloid suppressor cells represses NK cell cytotoxicity in tumor-bearing host. Blood 2007;109:4336–4342.
29 Nausch N, Galani IE, Schlecker E, Cerwenka A: Mononuclear myeloid-derived 'suppressor' cells express RAE-1 and activate natural killer cells. Blood 2008;112:4080–4089.
30 Zoglmeier C, Bauer H, Nörenberg D, Wedekind G, Bittner P, Sandholzer N, et al: CpG blocks immunosuppression by myeloid-derived suppressor cells in tumor-bearing mice. Clin Cancer Res 2011;17:1765–1775.
31 Shirota Y, Shirota H, Klinman DM: Intratumoral injection of CpG oligonucleotides induces the differentiation and reduces the immunosuppressive activity of myeloid-derived suppressor cells. J Immunol 2012;188:1592–1599.
32 Ebihara T, Azuma M, Oshiumi H, Kasamatsu J, Iwabuchi K, Matsumoto K, et al: Identification of a poly(I:C)-inducible membrane protein that participates in dendritic cell-mediated natural killer cell activation. J Exp Med 2010;207:2675–2687.
33 McCartney S, Vermi W, Gilfillan S, Cella M, Murphy TL, Schreiber RD, et al: Distinct and complementary functions of MDA5 and TLR3 in poly(I:C)-mediated activation of mouse NK cells. J Exp Med 2009;206:2967–2976.
34 Takeda K, Oshima H, Hayakawa Y, Akiba H, Atsuta M, Kobata T, et al: CD27-mediated activation of murine NK cells. J Immunol 2000;164:1741–1745.
35 Chan CJ, Andrews DM, Mclaughlin NM, Yagita H, Gilfillan S, Colonna M, et al: DNAM-1/CD155 interactions promote cytokine and NK cell-mediated suppression of poorly immunogenic melanoma metastases. J Immunol 2010;184:902–911.
36 Navabi H, Jasani B, Reece A, Clayton A, Tabi Z, Donninger C, et al: A clinical grade poly I:C-analogue (Ampligen) promotes optimal DC maturation and Th1-type T cell responses of healthy donors and cancer patients in vitro. Vaccine 2009;27:107–115.
37 Shojaei F, Wu X, Malik AK, Zhong C, Baldwin ME, Schanz S, et al: Tumor refractoriness to anti-VEGF treatment is mediated by CD11b+Gr1+ myeloid cells. Nat Biotechnol 2007;25:911–920.
38 Spits H, Artis D, Colonna M, Diefenbach A, Di Santo JP, Eberl G, et al: Innate lymphoid cells – a proposal for uniform nomenclature. Nat Rev Immunol 2013;13:145–149.
39 Arany I, Fleischmann CM, Tyring SK, Fleischmann WR: Interferon regulates expression of mda-6/WAF1/CIP1 and cyclin-dependent kinases independently from p53 in B16 murine melanoma cells. Biochem Biophys Res Commun 1997;233:678–680.
40 Ugel S, Delpozzo F, Desantis G, Papalini F, Simonato F, Sonda N, et al: Therapeutic targeting of myeloid-derived suppressor cells. Curr Opin Pharmacol 2009;9:470–481.

JVI
Journals.ASM.org

The Hepatitis E Virus Capsid C-Terminal Region Is Essential for the Viral Life Cycle: Implication for Viral Genome Encapsidation and Particle Stabilization

Tomoyuki Shiota, Tian-Cheng Li, Sayaka Yoshizaki, Takanobu Kato, Takaji Wakita, Koji Ishii
Department of Virology II, National Institute of Infectious Diseases, Gakuen, Musashi-murayama, Tokyo, Japan

Although the C-terminal 52 amino acids (C52aa) of hepatitis E virus (HEV) capsid are not essential for morphology, the C52aa-encoding region is required for replication. Transfection of a C52aa knockdown mutant showed transient growth, and the earliest population included a majority of noninfectious (possibly empty) particles and a minority of infectious particles with C-terminal capsid degradation. Finally, the complete revertant was generated reproducibly. C52aa is essential for the viral life cycle, promoting accurate encapsidation and stabilizing encapsidated particles.

Hepatitis E virus (HEV) is responsible for acute and enterically transmitted hepatitis in the developing world (1). Before the establishment of high-efficiency HEV cell culture systems (2), *in vitro* generation of HEV virus-like particles (HEV-VLPs) in insect cells and *in vivo* propagation in nonhuman primates were the most useful models for the study of HEV. Genetic deletions or cellular processing resulting in the loss of the N-terminal 111 or 13 amino acids (aa) or of the C-terminal 52 aa (C52aa) yielded capsid protein capable of directing the formation of the HEV small (S) or large (L) VLPs (3–5). Particle formation was required for C52aa abbreviation, limiting the structural analysis of the resulting particles (3, 4, 6–10). However, the contribution of the C52aa-encoding sequence was confirmed by both *in vivo* (attenuated infectivity of the point mutant virus in nonhuman primates) and *in vitro* (reduced RNA synthesis by RNA-dependent RNA polymerase [RdRp]) assays (11–14). Furthermore, the highly conserved nature of the C52aa sequence implies that the C52aa domain itself is functionally important. In this study, we characterized the role of the C52aa domain in the HEV life cycle by using infectious clones.

We constructed infectious clones by using the infectious virus G3-HEV83-2-27, employing a procedure described previously (20). Using a synthetic cDNA as the template, we amplified 12 fragments covering the entire G3-HEV83-2-27 genome by PCR with the primers listed in Table 1. These fragments were ligated stepwise and were inserted into the EcoRI-HindIII site of pUC19, yielding a wild-type clone that we designated WT. Site-directed mutagenesis of WT was used to generate clones that were mutated to encode capsid protein lacking the C52aa domain, either by introduction of an amber stop codon, UAA (a knockdown mutant designated Amut), or via deletion of the corresponding segment of the open reading frame 2 (ORF2) sequence (a knockout mutant designated Dmut). We performed experiments on three separate scales (normal, large, and huge, as described below) in order to estimate virus progeny productivity, to clarify the growth kinetics, and to analyze the process of encapsidation in the absence of revertants.

Normal scale. To estimate the virus progeny productivity of HEV without C52aa, transfection with Amut and Dmut was performed in comparison to transfection with WT. A 50-μg quantity of RNA from each infectious clone was electroporated into 1×10^7 cells of PLC/PRF/5. Analysis by enzyme-linked immunosorbent assay (ELISA) (using an anti-G3-HEV-VLP rabbit polyclonal antibody [5]) suggested that transient growth was observed with Amut, in contrast to continuous growth with WT (Fig. 1A) and no growth with Dmut (data not shown). The productivity (expressed as the genome copy number) of Amut, measured by real-time reverse transcription-PCR (RT-PCR) of RNA with a set of specific primers (Table 1), was estimated as approximately 40-fold lower than that of WT (Fig. 1B and 1C; note the differences in scale). However, subsequent analysis demonstrated that the Amut-derived HEV actually harbored synonymous and nonsynonymous reversion mutations, suggesting that the actual productivity (of intact Amut) was much lower than that suggested by real-time RT-PCR. To assess the progeny, sucrose density gradient analysis (SDGA) (with a gradient from 10 to 60% [wt/vol] sucrose) was performed. Subsequently, the collected fractions were separated by sodium dodecyl sulfate-polyacrylamide gel electrophoresis (SDS-PAGE), and Western blot analysis (WB) was performed with the polyclonal antibody noted above (5). Chemiluminescence was recorded using an LAS-3000 luminescent image analyzer (Fujifilm, Tokyo, Japan). In the series of fractions obtained from progeny derived from infection with WT, the presence of antigen was confirmed only in fraction 8 (F8) in Fig. 1C by WB (data not shown). The 72-kDa size of the prominent band was in agreement with the size of the capsid protein predicted for the WT clone. Quantification of the HEV RNA genome copy number showed a trailing peak for the progeny derived from infection with Amut (Fig. 1B, F8 and F9) and a single peak for the progeny derived from infection with WT (Fig. 1C, F8). These peaks corresponded to similar specific densities. Sequence analysis showed that while the progeny from infection with WT carried the original sequence, the progeny from infection with Amut did not contain the expected UAA (amber codon) at this position. Instead, the trailing peak of this Amut-derived sample corresponded to two

Received 12 February 2013 Accepted 22 February 2013
Published ahead of print 6 March 2013
Address correspondence to Koji Ishii, kishii@nih.go.jp.

doi:10.1128/JVI.00444-13

TABLE 1 Primers used for the construction of an HEV infectious cDNA clone, the C52aa deletion mutant, and the amber mutant and for the quantification and sequencing of HEV RNA by real-time RT-PCR

Name	Polarity[a]	Sequence (5′–3′)	Position in genome (nt)[b]	Amplicon (amplified region in genome [nt])[b]
ET7G2-F	+	GAATTCAATACGACTCACTATAGGCAGACCACGTATGTGGTCGAT[c]	2–23	Fragment 1-1 (2–155)
155R-EV	−	AGTCTGCACGCGAGATAAAAACGGCCGGAC	126–155	
126F-EV	+	GTCCGGCCGTTTTTATCTCGCGTGCAGACT	126–155	Fragment 1-2 (126–1370)
1370R-EV	−	CACCCTGGGATCCAGATGGAAGCCCGCAG	1342–1370	
1363F-EV	+	TCTGCGGGCTTCCATCTGGATCCCAGGGTG	1341–1370	Fragment 2-1 (1341–1794)
1816R-EV	−	ACTGCTCAGGGCCGTTCGCCTCAAGATGAG	1765–1794	
1787F-EV	+	CTCATCTTGAGGCGAACGGCCCTGAGCAGT	1765–1794	Fragment 2-2 (1765–2934)
2956R-EV	−	CGGCACAGGCACGGCCAACCTCTGTGGCAG	2905–2934	
2857F-EV	+	CCGATGCAGCCGGCACTCACAATAACGGAG	2835–2864	Fragment 3-1 (2835–3194)
3216R-EV	−	AGCCCGCTGCATATGTAATAGCAGCAAGTG	3165–3194	
3187F-EV	+	CACTTGCTGCTATTACATATGCAGCGGGCT	3165–3194	Fragment 3-2 (3165–3925)
3947R-EV	−	TCCGTAAGCTCAAAAACCAACACACTATCG	3896–3925	
3918F-EV	+	CGATAGTGTGTTGGTTTTTGAGCTTACGGA	3896–3925	Fragment 3-3 (3896–4598)
4620R-EV	−	CTTCCAAAACCCCTTAAGGGATTCCTTAGG	4569–4598	
4591F-EV	+	CCTAAGGAATCCCTTAAGGGGTTTTGGAAG	4569–4598	Fragment 4-1 (4569–5406)
5428R-EV	−	CTGTCGAGGGCGAGCTCCAGCCCCGGATTG	5377–5406	
5399F-EV	+	CAATCCGGGGCTGGAGCTCGCCCTCGACAG	5377–5406	Fragment 4-2 (5377–5851)
5873R-EV	−	TGGAGTTCATGTCAACAGAAGTAGGGGTAG	5822–5851	
5844F-EV	+	CTACCCCTACTTCTGTTGACATGAACTCCA	5822–5851	Fragment 4-3 (5822–6185)
6207R-EV	−	GTTCCATCGGCACCGCGGCGCAGCCGATG	6157–6185	
6179F-EV	+	CATCGGCTGCGCCGCGGTGCCGATGGAAC	6157–6185	Fragment 5-1 (6157–7101)
7101R-EV	−	AGTAGACTGGAAGGCGCAACCCTGC	7077–7101	
6981F-EV	+	CTGCGGTCGGTGTGTTAGCTCCACACTCGG	6959–6988	Fragment 5-2 (6959–7266)
SmartIIA-Hind	−	GCTCGAGCGGCCGCCAGTGTGATGGATATCTGCAGAATTCG GCTTAAGCAGTGGTATCAACGCAGAAAGCTTTTTTTTT TTTTTTTTTTTTTTTTTT[d]	7238–7266	
D81-F	+	ATGTGCCCTAGGGCTGTTCTGTTG	5173–5196	D81F/ORF2-52aa-Pac-R (5173–6995)
ORF2-52aa-Pac-R	−	AATTAATTAATTAAGCAAGGGCCGAGTGTGGAG[e]	6977–6995	
ORF2-52aa-del-F	+	TCCACACTCGGCCCTTGCTTAACTTGAGGATACTATTGACTAT[f]	6978–7020	
ORF2-52aa-del-R	−	ATAGTCAATAGTATCCTCAAGTTAAGCAAGGGCCGAGTGTGGA[f]	6978–7020	D81-F/ORF2-52aa-del-R (5173–7020)
7224R	−	AGGGAGCGCGAAAAGCAGAAAAGAAAAAT	7196–7224	ORF2-52aa-del-F/7224R (6978–7224)
HEV-G3-ANYF	+	ACCCCGGCAGTTGGTTTT	179–196	HEV-G3-ANYF/ANYR (179–234)
HEV-G3-ANYR	−	CCCGCTGGATAGGATGATTCC	212–234	
HEV-G3-ANYM1	+	FAM-CGCCCTGAGGTACTT-BHQ-1[g]	198–212	
83-2-6564F	+	GCTTCGTGCTAATGATGTTCTGTG	6564–6587	83-2-6564F/3′-terminal end (6564–7266)
83-2-6940F	+	CACCCAGGCTAGTGGTGTAGGTAGA	6940–6964	83-2-6940F/3′-terminal end (6940–7266)
ORF2-R-pacI	−	GAGAATTAAGACTCCCGGGTTTTAC	7136–7160	83-2-6564F/ORF2-R-pacI (6564–7160)

[a] Polarity of the primer on the HEV genome. +, forward; −, reverse.
[b] In G3-HEV83-2-27 (GenBank accession no. AB740232).
[c] The underlined sequence contains the T7 promoter.
[d] The underlined sequence contains a SmartIIA-specific sequence and a HindIII-digestible sequence.
[e] The underlined sequence contains a PacI-digestible sequence.
[f] The mutated nucleotides are underlined.
[g] The fluorophore 6-carboxyfluorescein (FAM) is attached to the 5′ end of the probe, and a quencher, Black Hole Quencher-1 (BHQ-1), is attached to the 3′ end.

distinct peaks (F8 and F9) harboring the GUU (Val-encoding) and GAC (Asp-encoding) codons, respectively. These changed RNA sequences were predicted to encode full-length revertant capsid proteins.

Large scale. To clarify the precise growth kinetics of Amut, a larger-scale transfection of Amut RNA was performed. Specifically, the large-scale transfection was performed on a scale approximately 30-fold larger than that described above, and culture supernatants were collected periodically. This procedure permitted a time course of quantification by ELISA analysis and showed that the peak of antigen accumulation occurred 25 days posttransfection, while the number of viral genomes progressively declined during the 2 months of the study (except for small recoveries in copy number on day 25 and at the end of the study) (Fig. 2A). These data suggested the production of a low level of infectious particles from Amut transfection. However, the nonreverted Amut antigens could not be distinguished by WB in the normal- and large-scale experiments, suggesting that the Amut products were unstable, of low infectivity, and/or produced in small amounts. To confirm the nature of the Amut product, pooled supernatants were subjected to partial purification and SDGA. WB of the resulting fractions detected a 72-kDa band in F7 (specific density, 1.15 g/ml) (Fig. 2B). Quantification of the HEV RNA genome in the fractions detected a single peak, primarily in F7 (Fig. 2C). Determination of the F7 sequence revealed that the codon expected to be an amber codon was instead GUC (complete reversion). Additionally, infection assays demonstrated that F7 readily infected cells (Fig. 2D). Based on our subsequent experiments, we suspect that the end product of the large-scale experiment likely corresponded to a revertant to WT.

Huge scale. To clarify the apparent reversion of Amut, transfection was performed at an even larger scale (10-fold increased over the large scale); culture supernatants were collected periodically, and viral sequences from these samples were determined. The results clearly showed a population shift from the originating amber codon of Amut to the complete revertant (GUC) via an intermediate mutant (GAC) (Table 2). Reversion mutants were

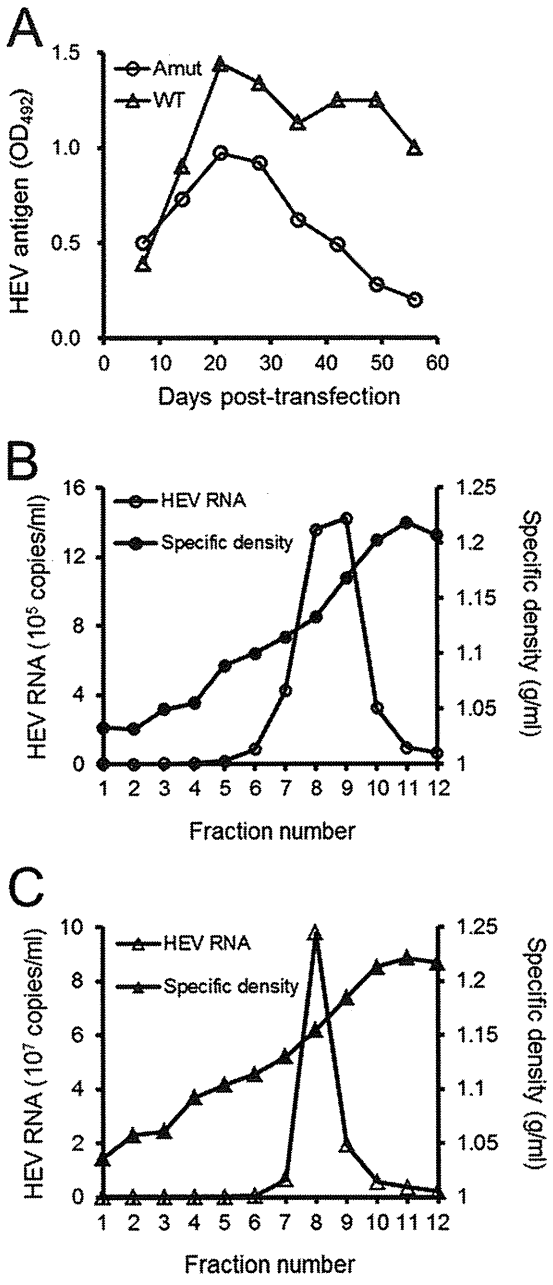

FIG 1 Initial characterization of Amut and WT HEV. (A) Time course of antigen production following transfection with Amut or WT HEV. HEV antigen levels were measured by ELISA using an anti-G3-HEV-VLP rabbit polyclonal antibody. OD_{492}, optical density at 492 nm. (B and C) Sedimentation analyses of the Amut product (B) and of the WT product, used as a control (C). Concentrated supernatants derived from 50-ml cultures were sedimented on continuous sucrose gradients (10% to 60% [wt/vol] in phosphate-buffered saline). The resulting fractions were assessed for specific density and the HEV RNA genome copy number (by real-time reverse transcription-PCR). Note the distinct *y*-axis scales in panels B and C.

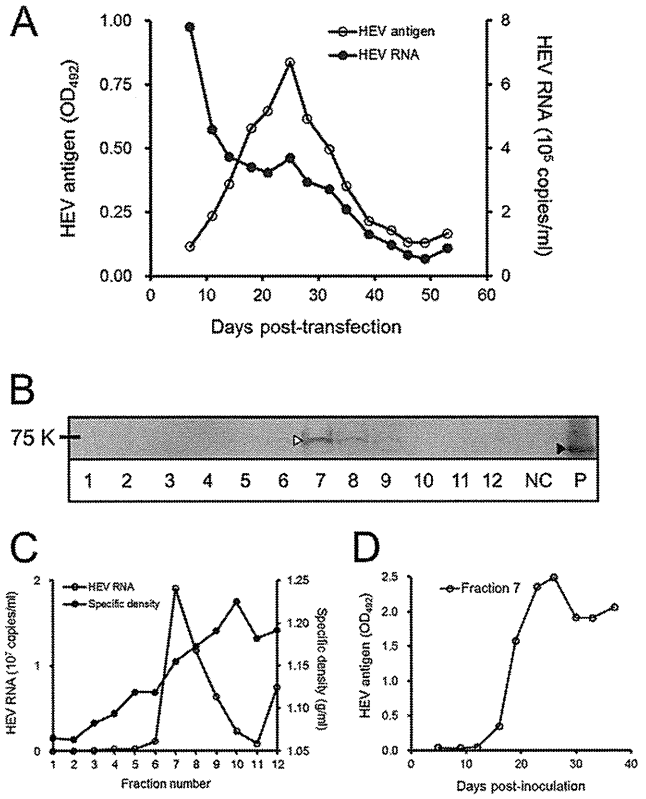

FIG 2 Growth kinetics and character of Amut. (A) Supernatants were collected periodically during 2 months of culturing, and HEV antigen levels were measured by ELISA using an anti-G3-HEV-VLP rabbit polyclonal antibody; the HEV RNA genome copy number was determined by real-time reverse transcription-PCR. OD_{492}, optical density at 492 nm. Supernatants from a pooled total of 3 liters of culture were concentrated and sedimented. (B) Fractions were subjected to Western blotting using an anti-G3-HEV-VLP rabbit polyclonal antibody. NC, negative control (untransfected cells). P, positive control (HEV-L-VLPs). 75 K, 75,000 (molecular weight). Symbols designate the positions of the major band in the Amut supernatant (open arrowhead) and the HEV-L-VLP (filled arrowhead). (C) Fractions were assessed for the HEV RNA genome copy number and specific density. (D) Confirmation of the infectivity of fraction 7 by ELISA.

not detected until 3 weeks posttransfection. The reproducible reversion of Amut provides evidence of the functional essentiality of the C52aa domain for the HEV life cycle.

To permit analysis of the Amut clone in the absence of revertants, culture supernatants collected within the first 10 days were pooled and subjected to partial purification and SDGA. WB detected multiple bands of approximately 55 kDa and smaller, starting in F7; these bands formed a broad range, with peak accumulation detected in F10 (specific density, 1.21 g/ml) (Fig. 3A). In contrast, F8 (specific density, 1.15 g/ml) had the highest copy number of the genome (Fig. 3B). For subsequent analysis, F8 and F10 were designated the minor and major products (Mip and Map, respectively) based on antigen levels. To determine the RNase sensitivities of the products, the fractions were treated with 20 μg/ml of RNase A for 30 min at 37°C. The RNase resistance of the fractions was confirmed by RT-PCR quantification analysis, indicating viral encapsidation. Both products exhibited resistance to RNase treatment (Fig. 3C), indicating the presence of encapsidated RNA. Neither the GAC nor the GUC reversion mutation was detected in these products by RT-PCR sequencing analysis, suggesting that those specific alleles were largely absent from this population.

Further analysis of peak discrepancy between the antigen level and the genome copy number revealed two points. First, the copy

TABLE 2 Time course sequence of the codon mutated to an amber codon for the supernatants of Amut-transfected cells

Codon	Sequence[a] at the following day posttransfection:								
	7	10	14	17	21	24	28	31	35
Amber mutant	UAA	UAA	UAA	UAA	UAA	ND	ND	ND	ND
Revertant									
Intermediate	ND	ND	ND	ND	ND	GAC	GAC	ND	ND
Complete	ND	ND	ND	ND	ND	GUC	GUC	GUC	GUC

[a] Determined for the first codon of the C52aa-encoding region of the ORF2 gene. ND, not detected.

number in the Map fraction was approximately 15 times lower than that in the Mip fraction (Fig. 3B). Second, the constitution (genome/antigen) ratio in the Map fraction was approximately 40-fold lower than that in the Mip fraction by analysis using Image Gauge, version 4.0 (Fujifilm, Tokyo, Japan); the ratio in the Mip fraction was approximately equal to that of WT (Fig. 3D). On the other hand, the RNA content of the Map fraction was extremely reduced, suggesting that these products represented empty parti-

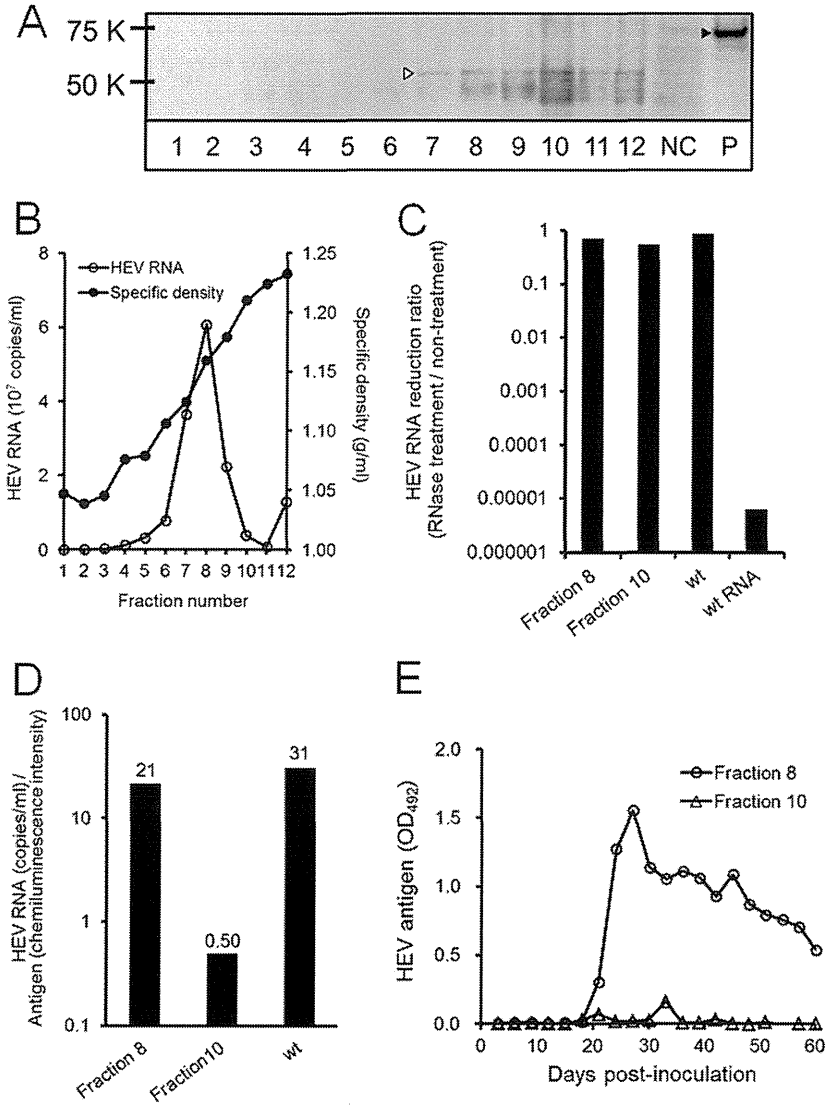

FIG 3 Encapsidation of the Amut genome and its characteristics. (A) Fractions were subjected to Western blotting using an anti-G3-HEV-VLP rabbit polyclonal antibody. NC, negative control (uninfected cells). Symbols indicate the positions of the major bands in the Amut fraction (55 kDa) (open arrowhead) and the WT fraction, used as a positive (P) control (72 kDa) (filled arrowhead). (B) Fractions were assessed for the HEV RNA genome copy number and specific density. (C) RNase resistance was measured as the ratio of the level of HEV RNA in RNase-treated fractions to that in untreated fractions (HEV RNA reduction ratio). WT virions and extracted WT RNA were used as positive and negative controls, respectively. (D) Constitution (genome/antigen) ratios (actual values are shown above the bars) were calculated by dividing the genome quantities from panel B by the chemiluminescence intensities from panel A. (E) To confirm the infectivity of the indicated fractions, cells were inoculated and periodically analyzed by ELISA using an anti-G3-HEV-VLP rabbit polyclonal antibody. OD_{492}, optical density at 492 nm.

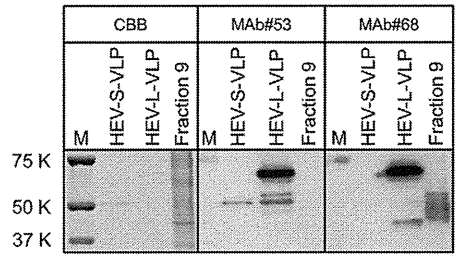

FIG 4 Detection of degraded capsid termini in Amut. HEV small virus-like particles (HEV-S-VLP), HEV large virus-like particles (HEV-L-VLP), and fraction 9 (derived as described for Fig. 3A) were stained with Coomassie brilliant blue (CBB) or were subjected to Western blot analysis using a monoclonal antibody specific to both HEV-S-VLP and HEV-L-VLP (MAb 53) or to HEV-L-VLP alone (MAb 68). Lane M, molecular weight markers.

cles; this inference is consistent with the low productivity of Amut products on all scales. Specifically, we observed that the Map fraction could not infect cells (Fig. 3E), while the Mip fraction was infectious for these cells (Fig. 3E) and yielded reversion mutants (GUC) during long-term observation (data not shown). While the viral reproduction of Amut was impaired, the Mip fraction could sustain low levels of viral production, leading to the emergence of revertants as shown in the large-scale experiment (Fig. 2A).

The observation, via WB (Fig. 3A), of a "smear" of antigen with a maximum size of 55 kDa was unexpected, given that the capsid protein lacking C52aa (predicted size, 6 kDa) was expected to migrate at 66 kDa (that is, 72 kDa less 6 kDa). The observed 11-kDa decrease in size suggested further degradation of the capsid in the absence of the C52aa domain. Mass spectroscopy followed by protein sequencing detected two fragments with amino acid sequences corresponding to early N-terminal capsid sequences. The presence of the capsid N-terminal domain was confirmed by detection with monoclonal antibody (MAb) 68 (Fig. 4), a reagent that exhibits specificity for HEV-L-VLP (specific to the N-terminal 13 to 111 aa) (T. C. Li, unpublished observations). In contrast, the protein was not detected using the HEV-S-VLP- and HEV-L-VLP-specific MAb 53 (Fig. 4), implying the absence of the S-and-L common region. Protein sequencing and reactivity with the HEV-VLP-specific antibodies strongly suggested that the 55-kDa bands correspond to proteolytic products generated by degradation from the C terminus on the viral surface, presumably via loss of the P domain. Further degradation (to lower-molecular-weight species) probably occurred after encapsidation, given that previous studies showed that this region was essential for dimerization and particle formation by the capsid (3, 15, 16).

HEV virions exhibit distinct buoyant densities in feces (1.26 to 1.27 g/ml) and in circulating blood (1.15 to 1.16 g/ml), differences that might be associated with their cellular membrane content (17). The density of the Amut Map fraction was higher than that of the Mip fraction. This result is inconsistent with the notion that the Map is an empty particle (18). The Amut Mip fraction had the specific density of membrane-associated virions, although the ORF3 (egress-related) protein was not detected in these particles, in contrast to WT particles (T. Shiota, unpublished observations) (19). We hypothesize that the correct encapsidation of Amut resulted in an enveloped particle lacking the ORF3 protein (Mip; density, 1.15 g/ml), whereas the incorrect encapsidation of Amut resulted in an nonenveloped and (usually) empty particle (Map; density, 1.21 g/ml), the density of which was intermediate between that of the membrane-associated virion (1.15 to 1.16 g/ml) and the nonenveloped filled virion (1.26 to 1.27 g/ml) (17).

In the present study, we showed that the C52aa domain of the HEV capsid was essential for the HEV life cycle, as confirmed by reproducible reversion at the amber mutation, which would otherwise truncate the C52aa domain. The presence of the C52aa domain promoted the accurate encapsidation of HEV and protected the particle from further C-terminal degradation. To clarify the involvement of the C52aa domain in neutralization, further studies (e.g., using a MAb specific for this region) will be required.

ACKNOWLEDGMENTS

We thank N. Sugiyama for excellent technical support and I. Shiota for helpful discussions and critical reading.

This work was supported in part by grants-in-aid from the Ministry of Health, Labor, and Welfare and the Ministry of Education, Culture, Sports, Science, and Technology, Japan.

REFERENCES

1. **Chandra V, Taneja S, Kalia M, Jameel S.** 2008. Molecular biology and pathogenesis of hepatitis E virus. J. Biosci. 33:451–464.
2. **Tanaka T, Takahashi M, Kusano E, Okamoto H.** 2007. Development and evaluation of an efficient cell-culture system for hepatitis E virus. J. Gen. Virol. 88:903–911.
3. **Li TC, Takeda N, Miyamura T, Matsuura Y, Wang JC, Engvall H, Hammar L, Xing L, Cheng RH.** 2005. Essential elements of the capsid protein for self-assembly into empty virus-like particles of hepatitis E virus. J. Virol. 79:12999–13006.
4. **Xing L, Li TC, Mayazaki N, Simon MN, Wall JS, Moore M, Wang CY, Takeda N, Wakita T, Miyamura T, Cheng RH.** 2010. Structure of hepatitis E virion-sized particle reveals an RNA-dependent viral assembly pathway. J. Biol. Chem. 285:33175–33183.
5. **Li TC, Yamakawa Y, Suzuki K, Tatsumi M, Razak MA, Uchida T, Takeda N, Miyamura T.** 1997. Expression and self-assembly of empty virus-like particles of hepatitis E virus. J. Virol. 71:7207–7213.
6. **Mori Y, Matsuura Y.** 2011. Structure of hepatitis E viral particle. Virus Res. 161:59–64.
7. **Xing L, Kato K, Li T, Takeda N, Miyamura T, Hammar L, Cheng RH.** 1999. Recombinant hepatitis E capsid protein self-assembles into a dual-domain T=1 particle presenting native virus epitopes. Virology 265:35–45.
8. **Guu TS, Liu Z, Ye Q, Mata DA, Li K, Yin C, Zhang J, Tao YJ.** 2009. Structure of the hepatitis E virus-like particle suggests mechanisms for virus assembly and receptor binding. Proc. Natl. Acad. Sci. U. S. A. 106:12992–12997.
9. **Yamashita T, Mori Y, Miyazaki N, Cheng RH, Yoshimura M, Unno H, Shima R, Moriishi K, Tsukihara T, Li TC, Takeda N, Miyamura T, Matsuura Y.** 2009. Biological and immunological characteristics of hepatitis E virus-like particles based on the crystal structure. Proc. Natl. Acad. Sci. U. S. A. 106:12986–12991.
10. **Xing L, Wang JC, Li TC, Yasutomi Y, Lara J, Khudyakov Y, Schofield D, Emerson SU, Purcell RH, Takeda N, Miyamura T, Cheng RH.** 2011. Spatial configuration of hepatitis E virus antigenic domain. J. Virol. 85:1117–1124.
11. **Agrawal S, Gupta D, Panda SK.** 2001. The 3′ end of hepatitis E virus (HEV) genome binds specifically to the viral RNA-dependent RNA polymerase (RdRp). Virology 282:87–101.
12. **Emerson SU, Zhang M, Meng XJ, Nguyen H, St Claire M, Govindarajan S, Huang YK, Purcell RH.** 2001. Recombinant hepatitis E virus genomes infectious for primates: importance of capping and discovery of a *cis*-reactive element. Proc. Natl. Acad. Sci. U. S. A. 98:15270–15275.
13. **Graff J, Nguyen H, Kasorndorkbua C, Halbur PG, St Claire M, Purcell RH, Emerson SU.** 2005. In vitro and in vivo mutational analysis of the 3′-terminal regions of hepatitis E virus genomes and replicons. J. Virol. 79:1017–1026.
14. **Kumar A, Panda SK, Durgapal H, Acharya SK, Rehman S, Kar UK.** 2010. Inhibition of hepatitis E virus replication using short hairpin RNA (shRNA). Antiviral Res. 85:541–550.

15. **Li SW, Zhang J, He ZQ, Gu Y, Liu RS, Lin J, Chen YX, Ng MH, Xia NS.** 2005. Mutational analysis of essential interactions involved in the assembly of hepatitis E virus capsid. J. Biol. Chem. **280**:3400–3406.
16. **Graff J, Zhou YH, Torian U, Nguyen H, St Claire M, Yu C, Purcell RH, Emerson SU.** 2008. Mutations within potential glycosylation sites in the capsid protein of hepatitis E virus prevent the formation of infectious virus particles. J. Virol. **82**:1185–1194.
17. **Takahashi M, Tanaka T, Takahashi H, Hoshino Y, Nagashima S, Jirintai, Mizuo H, Yazaki Y, Takagi T, Azuma M, Kusano E, Isoda N, Sugano K, Okamoto H.** 2010. Hepatitis E virus (HEV) strains in serum samples can replicate efficiently in cultured cells despite the coexistence of HEV antibodies: characterization of HEV virions in blood circulation. J. Clin. Microbiol. **48**:1112–1125.
18. **Jacobson MF, Baltimore D.** 1968. Morphogenesis of poliovirus. I. Association of the viral RNA with coat protein. J. Mol. Biol. **33**:369–378.
19. **Tyagi S, Korkaya H, Zafrullah M, Jameel S, Lal SK.** 2002. The phosphorylated form of the ORF3 protein of hepatitis E virus interacts with its non-glycosylated form of the major capsid protein, ORF2. J. Biol. Chem. **277**:22759–22767.
20. **Li T-C, Song S, Yang Q, Ishii K, Takeda N, Wakita T.** 2011. A cell culture system for hepatitis E virus. Hepatol. Int. **5**:202. doi:10.1007/s12072-010-9241-z.

Signal Peptidase Complex Subunit 1 Participates in the Assembly of Hepatitis C Virus through an Interaction with E2 and NS2

Ryosuke Suzuki[1]*, Mami Matsuda[1], Koichi Watashi[1], Hideki Aizaki[1], Yoshiharu Matsuura[2], Takaji Wakita[1], Tetsuro Suzuki[3]*

1 Department of Virology II, National Institute of Infectious Diseases, Tokyo, Japan, **2** Research Institute for Microbial Diseases, Osaka University, Osaka, Japan, **3** Department of Infectious Diseases, Hamamatsu University School of Medicine, Shizuoka, Japan

Abstract

Hepatitis C virus (HCV) nonstructural protein 2 (NS2) is a hydrophobic, transmembrane protein that is required not only for NS2-NS3 cleavage, but also for infectious virus production. To identify cellular factors that interact with NS2 and are important for HCV propagation, we screened a human liver cDNA library by split-ubiquitin membrane yeast two-hybrid assay using full-length NS2 as a bait, and identified signal peptidase complex subunit 1 (SPCS1), which is a component of the microsomal signal peptidase complex. Silencing of endogenous SPCS1 resulted in markedly reduced production of infectious HCV, whereas neither processing of structural proteins, cell entry, RNA replication, nor release of virus from the cells was impaired. Propagation of Japanese encephalitis virus was not affected by knockdown of SPCS1, suggesting that SPCS1 does not widely modulate the viral lifecycles of the *Flaviviridae* family. SPCS1 was found to interact with both NS2 and E2. A complex of NS2, E2, and SPCS1 was formed in cells as demonstrated by co-immunoprecipitation assays. Knockdown of SPCS1 impaired interaction of NS2 with E2. Our findings suggest that SPCS1 plays a key role in the formation of the membrane-associated NS2-E2 complex via its interaction with NS2 and E2, which leads to a coordinating interaction between the structural and non-structural proteins and facilitates the early step of assembly of infectious particles.

Citation: Suzuki R, Matsuda M, Watashi K, Aizaki H, Matsuura Y, et al. (2013) Signal Peptidase Complex Subunit 1 Participates in the Assembly of Hepatitis C Virus through an Interaction with E2 and NS2. PLoS Pathog 9(8): e1003589. doi:10.1371/journal.ppat.1003589

Editor: Aleem Siddiqui, University of California, San Diego, United States of America

Received February 1, 2013; **Accepted** July 19, 2013; **Published** August 29, 2013

Funding: This work was supported by a grant-in-aid for Scientific Research from the Japan Society for the Promotion of Science, from the Ministry of Health, Labour and Welfare of Japan and from the Ministry of Education, Culture, Sports, Science and Technology of Japan. The funders had no role in study design, data collection and analysis, decision to publish, or preparation of the manuscript.

Competing Interests: The authors have declared that no competing interests exist.

* E-mail: ryosuke@nih.go.jp (RS); tesuzuki@hama-med.ac.jp (TS)

Introduction

Over 170 million people worldwide are chronically-infected with hepatitis C virus (HCV), and are at risk of developing chronic hepatitis, cirrhosis, and hepatocellular carcinoma [1]. HCV is an enveloped virus of the family *Flaviviridae*, and its genome is an uncapped 9.6-kb positive-strand RNA consisting of the 5′ untranslated region (UTR), an open reading frame encoding viral proteins, and the 3′ UTR [2]. A precursor polyprotein is further processed into structural proteins (Core, E1, and E2), followed by p7 and nonstructural (NS) proteins (NS2, NS3, NS4A, NS4B, NS5A, and NS5B), by cellular and viral proteases. The structural proteins (Core to E2) and p7 reside in the N-terminal region, and are processed by signal peptidase from the polyprotein. NS2, NS3, and NS4A are prerequisites for proteolytic processing of the NS proteins. NS3 to NS5B are considered to assemble into a membrane-associated HCV RNA replicase complex. NS3 also possesses activities of helicase and nucleotide triphosphatase. NS4 is a cofactor that activates the NS3 protease. NS4B induces vesicular membrane alteration. NS5A is considered to play an important but undefined role in viral RNA replication. NS5B is the RNA-dependent RNA polymerase. It is now accepted that NS proteins, such as NS2, NS3, and NS5A, contribute to the assembly or release of infectious HCV [3–9].

NS2 protein is a transmembrane protein of 21–23 kDa, with highly hydrophobic N-terminal residues forming transmembrane helices that insert into the endoplasmic reticulum (ER) membrane [5,10]. The C-terminal part of NS2 resides in the cytoplasm, enabling zinc-stimulated NS2/3 autoprotease activity together with the N-terminal domain of NS3. The crystal structure of the C-terminal region of NS2 reveals a dimeric cysteine protease containing two composite active sites [11]. Prior work showed that NS2 is not essential for RNA replication of subgenomic replicons [12]; however, the protein is required for virus assembly independently of protease activity [5,6]. Several adaptive mutations in NS2 that increase virus production have been reported [13–17]. In addition, there is increasing evidence for genetic and biochemical interaction of NS2 with other HCV proteins, including E1, E2, p7, NS3-4A, and NS5A [10,18–25]. Thus, NS2 is now suggested to act as a scaffold to coordinate interactions between the structural and NS proteins for viral assembly. However, the molecular mechanism by which NS2 is involved in virus assembly remains unclear.

In this study, we identified signal peptidase complex subunit 1 (SPCS1) as a host factor that interacts with NS2 by yeast two-hybrid screening with a split-ubiquitin system. SPCS1 is a component of the microsomal signal peptidase complex which is